ACS OMEGA

http://pubs.acs.org/journal/acsodf

Article

Repurposing the Ebola and Marburg Virus Inhibitors Tilorone, Quinacrine, and Pyronaridine: *In Vitro* Activity against SARS-CoV-2 and Potential Mechanisms

Ana C. Puhl,* Ethan J. Fritch, Thomas R. Lane, Longping V. Tse, Boyd L. Yount, Carolina Q. Sacramento, Natalia Fintelman-Rodrigues, Tatyana Almeida Tavella, Fabio Trindade Maranhão Costa, Stuart Weston, James Logue, Matthew Frieman, Lakshmanane Premkumar, Kenneth H. Pearce, Brett L. Hurst, Carolina Horta Andrade, James A. Levi, Nicole J. Johnson, Samantha C. Kisthardt, Frank Scholle, Thiago Moreno L. Souza, Nathaniel John Moorman, Ralph S. Baric, Peter B. Madrid, and Sean Ekins*

Cite This: *ACS Omega* 2021, 6, 7454–7468

Read Online

ACCESS | Metrics & More | Article Recommendations | Supporting Information

ABSTRACT: Severe acute respiratory coronavirus 2 (SARS-CoV-2) is a newly identified virus that has resulted in over 2.5 million deaths globally and over 116 million cases globally in March, 2021. Small-molecule inhibitors that reverse disease severity have proven difficult to discover. One of the key approaches that has been widely applied in an effort to speed up the translation of drugs is drug repurposing. A few drugs have shown *in vitro* activity against Ebola viruses and demonstrated activity against SARS-CoV-2 *in vivo*. Most notably, the RNA polymerase targeting remdesivir demonstrated activity *in vitro* and efficacy in the early stage of the disease in humans. Testing other small-molecule drugs that are active against Ebola viruses (EBOVs) would appear a reasonable strategy to evaluate their potential for SARS-CoV-2. We have previously repurposed pyronaridine, tilorone, and quinacrine (from malaria, influenza, and antiprotozoal uses, respectively) as inhibitors of Ebola and Marburg viruses *in vitro* in HeLa cells and mouse-adapted EBOV in mice *in vivo*. We have now tested these three drugs in various cell lines (VeroE6, Vero76, Caco-2, Calu-3, A549-ACE2, HUH-7, and monocytes) infected with SARS-CoV-2 as well as other viruses (including MHV and HCoV 229E). The compilation of these results indicated considerable variability in antiviral activity observed across cell lines. We found that tilorone and pyronaridine inhibited the virus replication in A549-ACE2 cells with IC_{50} values of 180 nM and IC_{50} 198 nM, respectively. We used microscale thermophoresis to test the binding of these molecules to the spike protein, and tilorone and pyronaridine bind to the spike receptor binding domain protein with K_d values of 339 and 647 nM, respectively. Human C_{max} for pyronaridine and quinacrine is greater than the IC_{50} observed in A549-ACE2 cells. We also provide novel insights into the mechanism of these compounds which is likely lysosomotropic.

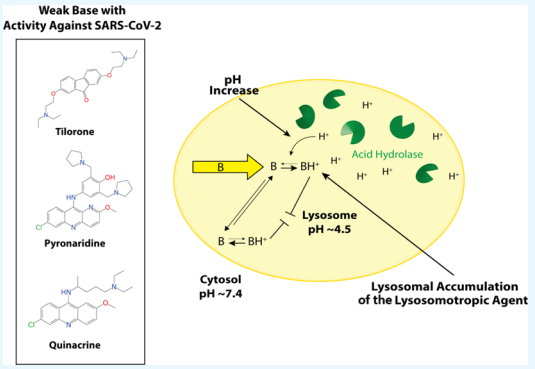

INTRODUCTION

As of March 2021, we remain in the midst of a global health crisis caused by a new virus that originated in Wuhan, China, in late 2019 and which has already generated unprecedented economic and social hardship. The new coronavirus, called severe acute respiratory coronavirus 2 (SARS-CoV-2) shares aspects of pathology and pathogenesis with the closely related SARS-CoV[1,2] and middle east respiratory syndrome coronavirus (MERS-CoV),[3] which also belong to the same family of *Betacoronavirus*. These viruses cause highly pathogenic respiratory infection that may lead to considerable morbidity, mortality, and the broad range of clinical manifestations associated with SARS-CoV-2, which has been collectively called 2019 coronavirus disease (COVID-19).[4] SARS-CoV-2 infection may result in cough, loss of smell and taste, respiratory distress, pneumonia, and extrapulmonary events characterized by a sepsis-like disease that require hospitalization and may lead to death.[5] Similar to SARS-CoV, SARS-CoV-2 directly interacts with the angiotensin converting enzyme 2 (ACE2) receptor in host cell types.[6−8] Because COVID-19 is established as a new

Received: December 9, 2020
Accepted: March 2, 2021
Published: March 10, 2021

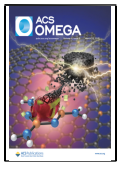

public health problem and vaccines are unlikely to eradicate animal reservoirs of SARS-CoV-2, inhibition of key events during the viral life cycle could pave the way for repurposed drugs.

Indeed, SARS-CoV-2 spread rapidly worldwide, prompting the World Health Organization to declare the outbreak a pandemic, with more than 1.5 million cases confirmed in less than 100 days. At the time of writing, there are over 116 million confirmed cases.[9] The high infection rate has caused considerable stress on global healthcare systems, leading to over 2.5 million deaths from COVID-19, and to date, USA has reported the largest number of fatalities.[9] Epidemic and pandemic disease outbreaks have intensified in recent years, and this will require various small-molecule therapeutic interventions to be developed.

There have been many efforts globally to screen and identify drugs for SARS-CoV-2, and there are currently clinical trials using existing drugs that are being repurposed. One early success was the RNA polymerase inhibitor remdesivir, which had previously been in a clinical trial for Ebola viruses (EBOVs),[10] while also demonstrating inhibition of MERS activity in rhesus macaques[11] and against many SARS-like coronaviruses, including SARS-CoV-2 in primary human cells and *in vivo*.[12,13] Remdesivir demonstrated activity in Vero cells,[13,14] human epithelial cells, and Calu-3 cells[13] infected with SARS-CoV-2, which justified further testing in the clinic. This drug was then the subject of numerous clinical trials globally.[15,16,49] These included a randomized double-blind, placebo-controlled multicenter trial that demonstrated that remdesivir reduced the days to recovery,[15] although adverse events were also higher in treated versus placebo groups. Regardless, it quickly received an emergency use authorization.[16] A recent double-blind, randomized, placebo-controlled trial in adults hospitalized with COVID-19 and who had evidence of lower respiratory tract infection demonstrated that remdesivir was superior to placebo in shortening the time to recovery.[49] Most recently, a large multicenter SOLIDARITY trial showed no efficacy for hospitalized patients with COVID-19, indicating that this drug may be more useful early in infection. This drug was also recently approved by the Food and Drug Administration (FDA) in October 2020.

There have also been notable failures, including hydroxychloroquine, which was also initially identified as active in Vero cells *in vitro*[17] but repeatedly failed completely in numerous clinical trials.[18,19]

Still, repurposing drugs represent possibly the fastest way to identify a drug and bring it to the clinic with fewer potential hurdles if it is already an approved drug or clinical candidate.[20,21] There have been several large-scale high-throughput screens; one used Huh-7 cells and tested 1425 compounds, identifying 11 with activity $IC_{50} < 1\ \mu M$.[22] Another screen of 1528 compounds led to 19 hits in Vero cells including 4 with IC_{50}s of $\sim 1\ \mu M$.[23] In addition, a screen of the Prestwick library in hPSC lung organoids identified three hits.[24] A total of 12,000 clinical stage or FDA-approved compounds in the ReFRAME library were also screened using Vero cells, which led to 21 hits.[25] To date, we have collated well over 500 drugs that have *in vitro* data from the various published *in vitro* studies against this virus[14,17,26,27] and used these to build a machine-learning model that was used to select additional compounds for repurposing and testing.[28] Several of these molecules had also previously demonstrated *in vitro* activity against EBOV. For example, a machine-learning model was previously used to identify tilorone, quinacrine, and pyronaridine tetraphosphate[54] (Figure 1), all of which had inhibited EBOV and Marburg *in vitro*, and they showed significant efficacy in the mouse-adapted EBOV (ma-EBOV) model.[29−32] All these molecules are also lysosomotropic,[33] which may contribute to their effect as possible entry inhibitors.

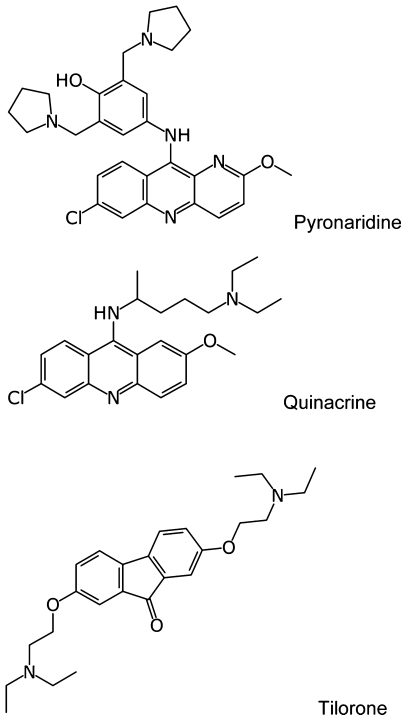

Figure 1. Structures of tilorone, quinacrine, and tilorone.

Both chloroquine and hydroxychloroquine, its hydroxyl derivative, are alkylated 4-aminoquinolines (4AQs).[34] Quinacrine has a side chain similar to that in chloroquine, but it is based on an acridine nucleus, which was the first known clinically tested antimalarial (Figure 1). This 9-aminoacridine was discovered in 1933 following an intensive search for synthetic quinine substitutes and was used when quinine became practically unavailable during World War II (WWII).[35] The nucleus of the drug pyronaridine is based on mepacrine (a 9-aminoacridine) with the addition of an amodiaquine-like side chain[35] (Figure 1). These antimalarials have been shown to be lysosomotropic. For chloroquine and hydroxychloroquine, this property causes 4AQs to accumulate within lysosomes and other intracellular acidic compartments due to protonation and sequestration of the drug.[34] Uncharged 4AQs readily diffuse into the lysosome, but once protonated at their two basic residues, they cannot diffuse back out into the cytoplasm.[34] Tilorone is an amphiphilic cationic compound and is found to increase lysosomal pH and inhibit the ATP-dependent acidification,[36] which are characteristics of being lysosomotropic, with an IC_{50} ($\sim 4\ \mu M$), on par with the well-known lysosomotropic compound chloroquine.[32] Quinacrine and pyronaridine have also been shown to be lysosomotropic.[37,38]

Pyronaridine tetraphosphate is currently used as an antimalarial in combination with artesunate (Pyramax) and has also shown significant activity in the guinea pig-adapted model of EBOV infection.[39] Tilorone is structurally different and is used in Eastern Europe as an antiviral for influenza.

https://dx.doi.org/10.1021/acsomega.0c05996
ACS Omega 2021, 6, 7454−7468

Tilorone has also demonstrated *in vitro* inhibition of MERS[32,40] and SARS-CoV-2 with a low μM IC_{50} in Vero cells.[26] Most recently, tilorone, quinacrine, and pyronaridine tetraphosphate were demonstrated to bind to the EBOV glycoprotein. The K_d values for pyronaridine (7.34 μM), tilorone (0.73 μM), and quinacrine (7.55 μM) possessed higher affinity than previously reported compounds that were found to bind to this protein.[33] All three compounds have therefore made it to the clinic in various parts of the world for other applications (e.g., malaria, influenza, antiprotozoal, and so forth) and represent molecules that could be viable candidates for testing in mouse-adapted models for SARS-CoV-2. We now describe our efforts to repurpose these molecules for SARS-CoV-2.

RESULTS

Cell Assays. SARS-CoV-2 susceptibility to tilorone, quinacrine, and pyronaridine was determined in two lineages of Vero Cells for initial screening. Unlike for Vero E6 (Figure S1) in the Vero 76 cell line (Table 1), tilorone emerged as a potential hit because of a 7.5-fold margin between cytotoxicity and potency, as judged by the selectivity index (SI) (Table 1). Moving forward to determine if these compounds were endowed with anti-SARS-CoV-2 activity in cells more relevant for COVID-19 pathophysiology, antiviral activity was assayed in intestinal, respiratory, hepatic, and immune cells. Testing in a virus yield reduction (VYR) assay on Caco-2 cells demonstrated activity for all three molecules (Table 2) with a quinacrine EC_{90} of 10.54 μM (CC_{50} 229.15 μM), a tilorone EC_{90} of 28.96 μM (CC_{50} 111.49), and a pyronaridine EC_{90} of 5.49 μM (CC_{50} 51.65 μM). For comparison purposes for efficacy across multiple cell lines, these data are depicted in Figure 2.

Table 1. EC_{50} and CC_{50} Values for Quinacrine, Pyronaridine, and Tilorone against SARS-CoV-2 (Strain USA_WA1/2020) in Vero 76 Cells[a]

compound	drug assay name	EC_{50} (μM)	CC_{50} (μM)	SI50
quinacrine hydrochloride	visual (CPE/toxicity)	>7.33	7.33	0
quinacrine hydrochloride	neutral red (CPE/toxicity)	>6.87	6.87	0
tilorone dihydrochloride	visual (CPE/toxicity)	6.62	49.64	7.5
tilorone dihydrochloride	neutral red (CPE/toxicity)	6.62	49.64	7.5
pyronaridine tetraphosphate	visual (CPE/toxicity)	>3.52	3.52	0
pyronaridine tetraphosphate	neutral red (CPE/toxicity)	>3.85	3.85	0

[a]Drug concentration range: 0.1−100 μg/mL.

Table 2. EC_{90} and CC_{50} Values for Quinacrine and Tilorone against SARS-CoV-2 (Strain USA_WA1/2020) in Caco-2 Cells[a]

compound	EC_{90} (μM)	CC_{50} (μM)	SI
quinacrine hydrochloride	10.54	229.15	>22
tilorone dihydrochloride	28.96	111.49	3.9
pyronaridine tetraphosphate	5.49	51.65	9.4

[a]Drug concentration range: 0.032−100 μg/mL. No CPE was observed in this assay. Only VYR data were reported.

By means of measuring the double-stranded virus RNA as a proxy of virus replication, tilorone showed activity in Calu-3 cells with an EC_{50} of 10.77 μM and selectivity index (SI) = 2 (Figure S2). For comparison, remdesivir showed an EC_{50} of 0.016 μM and an SI > 622 (Figure S2).

Tilorone was also tested in another laboratory (Dr. Thiago Moreno, Fiocruz, Brazil) at the multiplicity of infection (MOI) of 0.1 for 1 h at 37 °C and at different concentrations. Lysis of the cell monolayer was performed 48 h post infection, and the virus was titrated by plaque-forming unit (PFU) assays and reported as % inhibition. In this assay, tilorone had an IC_{50} of ∼9 μM and remdesivir showed almost 100% inhibition PFU/mL even at the lowest concentration tested of 0.6 μM [Figure S3, reported as % inhibition (A) and PFU/mL (B)].

SARS-CoV-2 can infect human hepatoma lineage (Huh-7); however, the viral titers produced in this cell are lower than those in Vero and Calu-3.[41] While African green monkey kidney cells (Vero E6), human hepatoma (HuH-7), and airway epithelial cells (Calu-3)[42] produced infectious SARS-CoV-2 titers and quantifiable RNA levels, A549 pneumocytes and induced pluripotent human neural stem cells displayed limited ability to generate virus progeny, as measured by PFUs of the virus below the limit of detection. In human hepatoma lineage (Huh-7), tilorone was tested and it did not show antiviral activity up to 1 μM (Figure S4).

Tilorone was also tested for its ability to impair SARS-CoV-2 replication in human primary monocytes at 10 μM. Human primary monocytes were infected at the indicated MOI of 0.1 and treated with 10 μM of tilorone or remdesivir for 24 h. Remdesevir showed almost 50% inhibition of SARS-CoV-2 measured by the cell-associated viral RNA levels quantified by real-time polymerase chain reaction (RT-PCR), when cells were treated with 10 μM of compounds (Figure S5A). The activity of tilorone (Figure S5A) was due to cytotoxicity (Figure S5B), and SI = 0. Quinacrine and pyronaridine were tested on MTT Cytotoxicity assays in human monocytes and Vero CCL81 cells and demonstrated similar CC_{50} (Figure S6).

The most promising results by far were achieved in A549-ACE2 cells which support SARS-CoV-2 growth to about 10^7 PFU/mL and in which quinacrine, tilorone, and pyronaridine all showed SARS-CoV-2 inhibition demonstrating IC_{50} values <200 nM (Figure 3) and good selectivity indices. This inhibition compares well with remdesivir under the same conditions. When cells were pretreated for 1 h with pyronaridine and tilorone prior to the infection step, the compounds showed a higher affinity (2−3 times) compared to incubation (when the virus was incubated with compounds for 1 h prior to adding to the cells) (Figure 3).

All three compounds were also tested against a group 2a murine hepatitis virus (MHV) in DBT cells, a model of betacoronavirus genetics and replication.[43] Quinacrine showed an IC_{50} of 2.3 μM, and pyronaridine showed an IC_{50} of 2.75 μM, while for tilorone, the dose response curve did not reach the plateau and the IC_{50} was estimated to be 20 μM (Figure 4).

These compounds were also tested in Huh-7 cells infected by the human coronavirus 229E (HCov-229E), a group A alphacoronavirus which infects humans and bats.[44,45] It is an enveloped, positive-sense, single-stranded RNA virus which enters its host cell by binding to the aminopeptidase N (AP-N) receptor.[46] Quinacrine showed a decrease of 3.9 logTCID50/mL when tested at 10 μM; pyronaridine showed a decrease of 2.83 logTCID50/mL when tested at 20 μM, and tilorone did not show significant inhibition. The CC_{50} was >15 μM for

https://dx.doi.org/10.1021/acsomega.0c05996
ACS Omega 2021, 6, 7454−7468

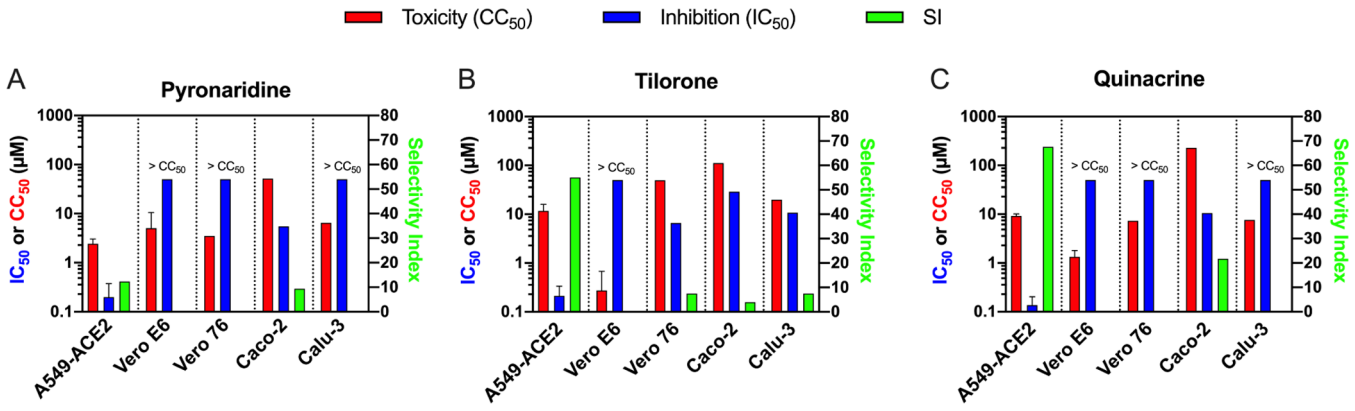

Figure 2. Synopsis of the efficacy of the inhibition of SARS-CoV-2 across the multiple cell lines assessed for pyronaridine (A), tilorone (B), and quinacrine (C). For simplicity, if no inhibition was able to be determined (i.e., $IC_{50} > CC_{50}$), these values were arbitrarily set to 50 μM as placeholders. Error bars (A549-ACE2 and Vero 76 only) represent the 95% CI.

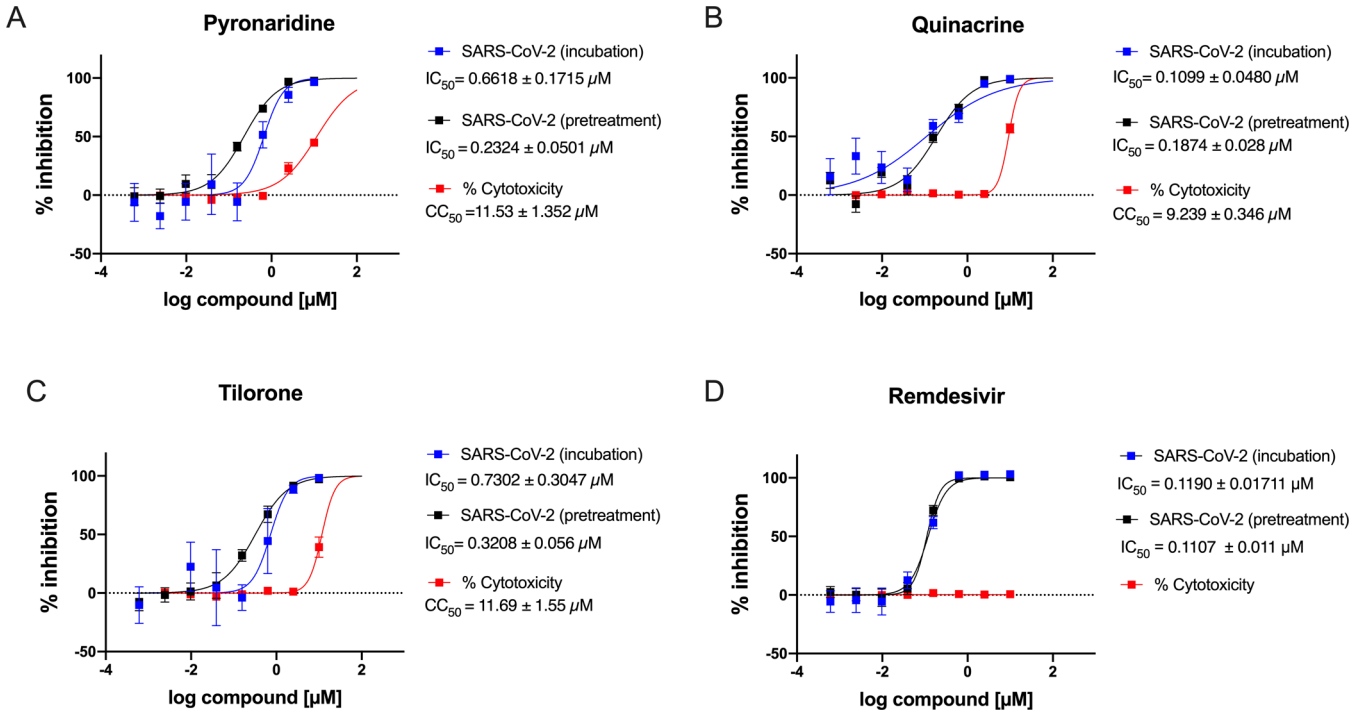

Figure 3. SARS-CoV-2 inhibition in A549-ACE2 cell lines. For each compound, inhibition was assessed with either an "incubation" (the virus and compound incubated for 1 h prior to infection) or "pretreatment" (cells incubated with the compound for 1 h prior to infection) step. Error bars for each point as well as the calculated IC_{50}s are shown with their respective SEM. Each point represents a minimum of six replicates. (A) Pyronaridine, (B) quinacrine, (C) tilorone, and (D) remdesivir.

quinacrine, and the CC_{50} was >20 μM for pyronaridine (Figure S7).

Microscale Thermophoresis. Based on our previous work showing that pyronaridine, tilorone, and quinacrine bind to EBOV glycoprotein,[33] this provided impetus to test them against the SARS-CoV-2 spike receptor binding domain (RBD). The K_d values for tilorone and pyronaridine were 339 and 647 nM, respectively, at pH 7.4 (Figure 5A) and 631 and 618 nM at pH 5.2, respectively (Figure 5B). Quinacrine did not demonstrate reproducible binding to this protein.

Vesicular Stomatitis Virus-Pseudotype SARS-CoV-2 Neutralization Assays. To directly measure the impact of these drugs on SARS-CoV-2 S glycoprotein-mediated entry, we employed vesicular stomatitis virus (VSV)-pseudotype SARS-CoV-2 assays. The neutralization activity for tilorone and pyronaridine did not achieve 50% neutralization as the dose response curves did not reach the plateau, suggesting little if any activity against SARS-CoV-2 spike protein-mediated docking and entry (Figure S8 and Table S2).

DISCUSSION

Identifying drugs for any new virus in real time is extremely challenging due to the pressure to identify a treatment while large numbers of patients are suffering or dying, with only palliative care available. The SARS-CoV-2 outbreak is only the most recent such example. In humans, SARS-CoV-2 is currently thought to cause a biphasic disease characterized by early high titer virus replication in airway epithelial cells and type II pneumocytes, followed by virus clearance and immune-mediated pathology.[47] Consequently, drug development against

https://dx.doi.org/10.1021/acsomega.0c05996
ACS Omega 2021, 6, 7454−7468

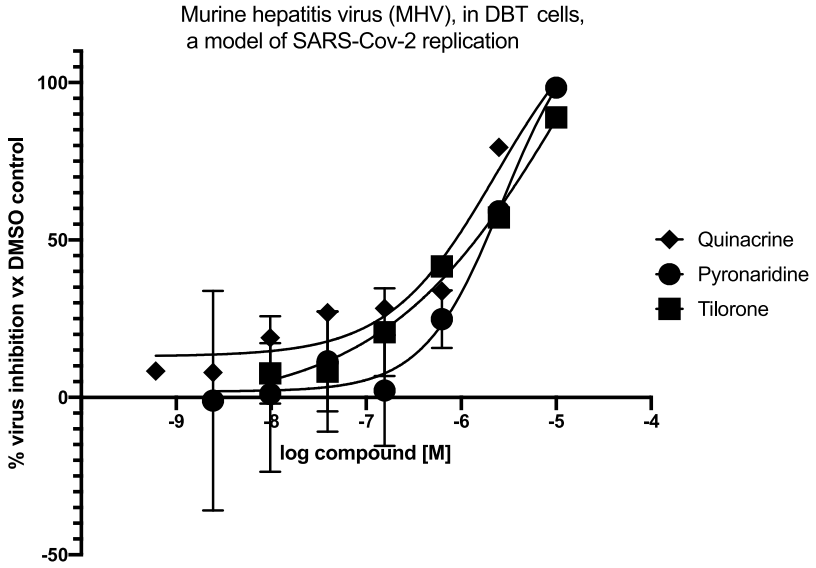

Figure 4. MHV in DBT cells, a model of SARS-Cov-2 replication. Quinacrine IC_{50} = 2.3 μM and pyronaridine IC_{50} = 2.75 μM. The tilorone dose response curve did not reach the plateau, and the IC_{50} was estimated to be 20 μM.

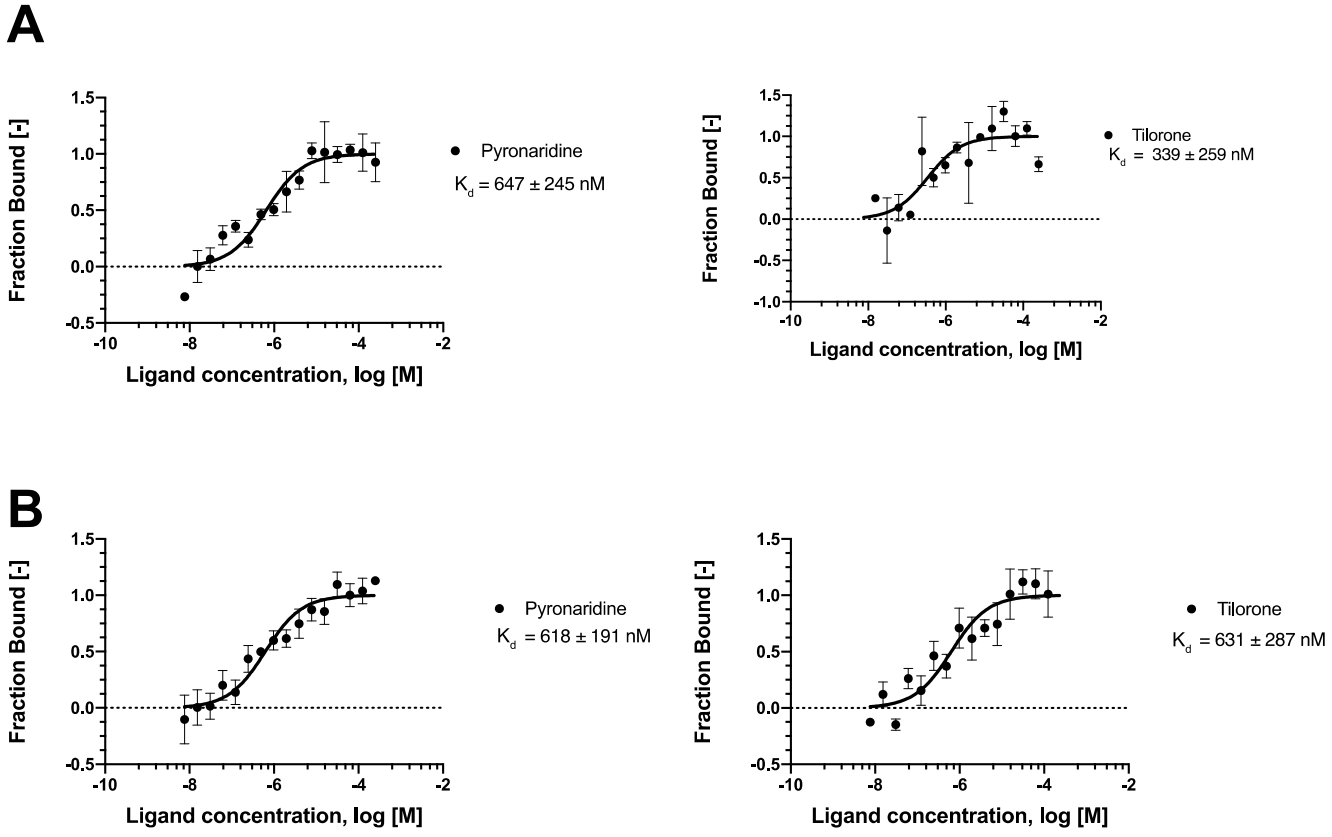

Figure 5. MST binding analysis for the interaction between spike RBD and compounds. The concentration of labeled spike RBD is kept constant at 5 nM, while the ligand concentration varies from 250 μM and 7.629 nM. The serial titrations result in measurable changes in the fluorescence signal within a temperature gradient that can be used to calculate the dissociation constant. The curve is shown as fraction bound [-] against compound concentration on a log scale. The binding affinity was measured at pH 7.4 (A) and pH 5.2 (B).

SARS-CoV-2 is complicated by the diverse disease-mediating mechanisms associated with early direct virus cell killing and late immune-mediated pathology.[47] Studies in animals and in humans demonstrate that early administration of direct-acting antivirals is essential for efficacy; however, later in infection combination therapies including direct-acting antivirals with anti-inflammatory drugs will likely be required. Most of the research emphasis to date has been on the development of vaccines (with several now approved) or biologics, and only a relatively few small molecules have made it to the clinic, such as remdesivir.[48,49] Remdesivir was originally developed for hepatitis C viruses (HCVs) and then repurposed for EBOV; therefore, we hypothesized that other drugs used for treating this latter virus should also be evaluated. Our focus on repurposing

https://dx.doi.org/10.1021/acsomega.0c05996
ACS Omega 2021, 6, 7454−7468

drugs for EBOV[54] previously has led us to apply our approaches to SARS-CoV-2.[28] We reasoned that the three molecules (pyronaridine, tilorone, and quinacrine) for which we already had some antiviral knowledge of may be a useful starting point to explore for repurposing for SARS-CoV-2 and, based on our results, further suggest that these compounds should be evaluated in SARS-CoV-2 mouse models.

Several groups have now published on these three drugs;[49,50] pyronaridine[51] and tilorone[26,52] are in clinical trials in different countries for SARS-CoV-2. Tilorone was previously identified *in vitro* in Vero cells as a hit against SARS-CoV-2 (IC_{50} 4 μM)[26] and has also been shown to have similar activity against MERS[41] and Ebola[53] (as has remdesivir[11]). Tilorone was recently found to block the endocytosis of preformed α-Syn fibrils and was an inhibitor of heparan sulfate proteoglycan (HSPG)-dependent endocytosis.[54] Combined with our earlier findings of tilorone binding to the EBOV glycoprotein,[33] this would suggest that at minimum a partial direct antiviral effect rather than an effect on the innate immune system (as long assumed since the 1970s)[32] is responsible for the efficacy observed in this case. In our hands, tilorone has also shown antiviral activity against SARS-CoV-2 in A549-ACE2 (IC_{50} 180 nM), in Vero 76 cell lines (IC_{50} of 6.62 μM) but not Vero E6, and to a lesser extent in Caco-2 and Calu-3.

Pyronaridine is used in combination with artesunate to treat malaria.[55] We have previously demonstrated that both molecules show additivity against EBOV.[56] Pyronaridine was therefore of interest to us as a potential antiviral against SARS-CoV-2. More recently, pyronaridine was tested again in Vero cells by others (IC_{50} 1.08 μM, CC_{50} 37.09 μM) at 24 hpi and in Calu-3 cells (IC_{50} 6.4 μM, CC_{50} 43.08 μM) at 24 hpi.[50] Our results do not match any of these earlier data as we showed no activity in Vero 76, Vero E6 cells, and Calu-3 cells, while we did see activity in Caco-2 (EC_{90} 5.49 μM), A549-ACE2 cells (IC_{50} = 198 nM), and MHV (IC_{50} 2.75 μM).

A recent screen of the Prestwick library in hPSC lung organoids identified the antiprotozoal quinacrine (EC_{50} 2.83 μM)[57] which was followed up in mice infected with the SARS-CoV-2 pseudovirus and showed a significant decrease in infected cells.[57] Others have not observed significant *in vitro* SARS-CoV-2 activity for quinacrine in Vero cells,[26] while it has previously been demonstrated to possess activity against Ebola-infected HeLa cells[53] but not Vero cells.[29] In this study, we confirm no *in vitro* activity in Vero E6, Vero76, and Calu-3 but demonstrate activity in Caco-2 (EC_{90} 10.54 μM), A549-ACE2 (IC_{50} 122 nM), and MHV (IC_{50} 2.3 μM) for quinacrine.

These three drugs have therefore shown considerable variability in testing in different cell types infected with SARS-CoV-2 (Table S1) as compared to the recent literature. The differences between these and previous data published in Vero cells could be due to a number of factors including differences in assays, MOI, time of addition of the drug and expression levels of ACE2. It should also be clear that we see differences in the data reported for these compounds as well. These three drugs have all demonstrated low μM activity against SARS-CoV-2 in the best cases, and while A549-ACE2 appears especially sensitive to these drugs, the effectiveness of the remdesivir control is in line with published data from different cell lines.[13] Our observations of no inhibition in Vero E6 cells for tilorone, quinacrine, and pyronaridine are exactly as we had observed previously for EBOV.[58] The gold standard currently is primary human airway epithelial cells or a primary type II ATII cell as are targeted by the virus *in vivo*.

We characterized binding of pyronaridine and tilorone to the spike RBD using microscale thermophoresis (MST), with K_d values for tilorone and pyronaridine of 339 and 647 nM, respectively (Figure 5). Pyronaridine and tilorone bind to the spike RBD with 20−40 times weaker affinity when compared to ACE2, which has been reported to be ∼15 nM by different techniques.[59,60] In the VSV-pseudotype SARS-CoV-2 neutralization assay, we saw no measurable activity for tilorone and pyronaridine (Figure S6 and Table S2), suggesting that it may be necessary to modify these compounds to increase affinity for the spike protein to enhance activity. The binding affinity experiments using MST were performed with the RBD, which is the RBD that binds to ACE2. Despite these compounds binding to the spike RBD, their affinity is clearly not high enough to compete with binding to ACE2 in the pseudovirus assay and the compounds may bind to the RBD in a location that does not affect binding to the ACE2 receptor. We have previously characterized that these compounds are lysosomotropic,[56] so this may also be their mechanism of action against SARS-CoV-2, but this will require a significant amount of work outside the scope of this paper to confirm.

The effect of lysosomotropic compounds on cells is multifaceted as evidenced by the prototypical lysosomotropic compound chloroquine. A well-known antiviral effect of chloroquine is against EBOV and has been associated with the pH increase within lysosomes, which reduces the efficiency of acid hydrolases (cathepsins) required for viral glycoprotein priming.[61] As there is some evidence that cathepsin is also involved in one entry mechanism of SARS-CoV-2, this function may also be involved in the partial inhibition of SARS-CoV-2 by compounds of this class, although it is unlikely the only mechanism of inhibition by lysosomotropic compounds. Interestingly, SARS-CoV-2 has recently been shown to also increase the pH of lysosomes, possibly through the open reading frame protein 3A (ORF3a).[62] As the sarbecovirus E protein also functions as a viroporin, these overlapping activities are likely requisites for efficient SARS-CoV-2 infection.[63−66] ORF3a has been shown to traffic to lysosomes and disrupt their acidification and ultimately viral egress.[62] ORF3a is also a viroporin, which modifies several cellular functions, including membrane permeability, membrane remodeling, and glycoprotein trafficking.[67] While lysosomotropic compounds have been shown to increase lysosomal pH, this effect has been demonstrated to be transient with multiple lysosomotropic compounds including chloroquine, fluoxetine, tamoxifen, and chlorpromazine. This was illustrated by multiple types of measurements, including a lack of a decrease in cathepsin activity over time.[68] It is possible that since cells are able to counter the pH change caused by the lysosomotropic compounds, this may translate into this same phenomenon with SARS-CoV-2-infected cells. If an increased pH of the lysosome is indeed required for the efficient egress of the virus, compounds that counteract this would potentially act as an antiviral. The "redundant" viroporin activities of E protein and ORF3a may also complicate the specificity and potency of lysosomotropic compounds if they target one but not both proteins. This is consistent with the ability to delete either one separately and still have a viable virus, yet if both are deleted, then the virus is inhibited. Consequently, lysosomotropic inhibitors must target both activities.

While a pH change in acidic organelles is the most well-known effect of lysosomotropic compounds, they are also known to elicit other cellular effects such as inducing vacuole formation[69,70] by the fusion of lysosomes and late endosomes.[71]

https://dx.doi.org/10.1021/acsomega.0c05996
ACS Omega 2021, 6, 7454−7468

This is an important distinction because a precursor to this is a general disorganization of the Golgi complexes with an increased number of vesicles found proximal to the Golgi.[70] Therefore, lysosomotropic compounds not only create vacuoles but also cause the disruption of vesicle translation from the Golgi to distal subcellular locations.[72−74] Many lysosomotropic compounds have shown a similar disruption in vesicle trafficking, including transport to the apical plasma membrane.[75,76] Disruption of this translocation of vesicles from the trans golgi network (TGN) would likely inhibit the common biosynthetic secretory pathway used for egress of multiple viruses such as HCVs, dengue viruses, and West Nile viruses.[77,78] Additionally, many drugs that are known to be lysosomotropic also induce phospholipidosis in cells,[79] which is the reduced degradation of phospholipids, causing an excess accumulation in cells. The mechanism of drug-induced phospholipidosis is unclear but could be due to the cationic drug binding to bis(monoacylglycero)phosphate (BMP) in the phospholipid bilayer, which is heavily enriched within the lysosome membrane.[80] This affects the efficiency of acid hydrolases as well as disrupts interactions between membrane-bound proteins and molecules within the lysosomal lumen. Drug-induced phospholipidosis is also suggested to alter the lysosomal membrane curvature[81] similar to pH.[82] A change in membrane curvature is a phenomenon suggested to be important for the membrane fusion of other viruses,[83] which points to a similar effect on the membrane fusion of SARS-CoV-2. Multiple cellular alterations by lysosomotropic compounds may be involved in the inhibition of SARS-CoV-2 egress.

Despite the compounds binding to the RBD, the affinity is 20−40 times lower as compared to binding to ACE2. Figure 3 shows that when cells were pretreated for 1 h with pyronaridine and tilorone prior to the infection step, the compounds showed a higher affinity (2−3 times) compared to incubation (when the virus was incubated with compounds for 1 h prior to adding to the cells). This supports the hypothesis that the mechanism relies more on a host effect than on an effect on the virus, which further supports one of the mechanisms we proposed, specifically the lysosomotropic aspect of the compounds. It has also been demonstrated that the uptake of weak bases into lysosomes is a progressive process, which may take 20−60 min or longer to go to completion,[1] so a longer pretreatment time may show various effects. The difference in inhibition between incubation and pretreatment is statistically significant for both tilorone and pyronaridine. Pyronaridine and tilorone are stronger lysosomotropic compounds than quinacrine, which is based on their ability to inhibit lysotracker red.[56] This could be one explanation why pretreatment with tilorone and pyronaridine has lower IC_{50}s than those with incubation (virus + compound) and why this does not occur with quinacrine.

The relevance of pyronaridine, tilorone, and quinacrine as antivirals can be further assessed using their concentrations attained *in vivo*. The C_{max} data in our previous mouse pharmacokinetics studies (intraperitoneal dosing) suggests that the concentration is above the average IC_{50} observed for EBOV inhibition *in vitro* (∼1 μM) (Table S2). For quinacrine and pyronaridine, we have also identified published human pharmacokinetics data, and these suggest that IC_{50} values up to 1 μM would be below the C_{max} achieved for quinacrine and pyronaridine (Table S3). Therefore, as we have demonstrated IC_{50} values in some cell lines infected with SARS-CoV-2 around or below 1 μM this may enable them to achieve efficacious concentrations. While we could not find human pharmacokinetics data for quinacrine, it can still be considered as it was safely used during WWII in millions of soldiers as an antimalarial.[29] These three molecules generally have excellent *in vitro* ADME properties, and there is a considerable body of data that we have built up on them (Table S4) including the maximum tolerated dose in mice. This would certainly be useful for designing efficacy assessment studies in SARS-CoV-2-infected mouse models in future.

It is important to study virus infection in different cell lines and understand the subtle differences among them when treated with drugs. SARS-CoV-2 infection experiments using primary human airway epithelial cells have been found to have CPEs 96 h after the infection.[84] However, primary human airway epithelial cells are expensive and do not proliferate indefinitely.[85] Several infinitely proliferating cell lines, such as Caco-2,[86] Calu-3,[87] HEK293T,[88] and Huh7,[87] have been utilized in SARS- CoV-2 infection experiments. These cell lines do not accurately mimic human physiological conditions and generate low titers of infectious SARS-CoV-2.[86−88] Despite this limitation, valuable information about the virus infection and replication can be learned from studies using these cell lines. A previous study[89] assessed 25 cell lines derived from different tissues or organs and host species and reported that CPEs were only seen in VeroE6 and FRhK4 cells after SARS-CoV-2 inoculation for up to 120 hpi. These findings are important for optimization of antiviral assays based on cell protection assessment because cell lines without obvious CPEs might lead to overestimation of cell viability and drug efficacy.[89] For efficient SARS-CoV-2 research, a cell line, such as Vero cells, that can easily replicate and isolate the virus is essential, but they have been shown not to produce interferons (IFNs) when infected with Newcastle disease viruses, rubella viruses, and other viruses.[90] Under previously described experimental conditions, productive SARS-CoV-2 replication in A549 cells was erratic,[41] which can be overcome by preparing A549 cells overexpressing ACE2 (as used in the current study).

The differences in responses in different cell lines could be accounted for by the basic biochemistry, for example, hepatic cells, like Huh-7, are equipped with enzymes to synthesize nucleotides, carbohydrates, and lipids.[91] Hence, it is not surprising that the highest potency of remdesivir against SARS-CoV-2 is found in Huh-7 cells, followed by Calu-3 and Vero, implying that Huh-7 and subsequently Calu-3 are active to convert it to its triphosphate.[41,92]

SARS-CoVs that enter the host via the respiratory tract, airway and alveolar epithelial cells, vascular endothelial cells, and alveolar macrophages are among their first targets of viral entry.[93] Viral entry may depend as well on the expression of TMPRSS2 because nearly undetectable amounts of ACE2 still support SARS-CoV entry as long as TMPRSS2 is present.[94] The SARS-CoV-2 spike contains a furin cleavage site, thus reducing the dependence of SARS-CoV-2 on target cell proteases (TMPRSS2/cathepsin L) for entry,[95,102] and furin is abundantly expressed in human bronchial epithelial cells, thus potentially extending its cellular tropism.[96]

While the nasal airway epithelium replicates the virus best early,[97] Type II pneumocytes are the most affected cells in the lung of patients that died from COVID-19.[98] Both A549 and Calu-3 cells are lung epithelial cells (based on ATCC information). Under continuous submersible culture, A549 cells decrease the expression of the type C surfactant and enhances the expression of aquaporin V, a phenotype of type I pneumocytes.[99] Calu-3 is an airway epithelial cell that can be

https://dx.doi.org/10.1021/acsomega.0c05996
ACS Omega 2021, 6, 7454−7468

induced to differentiate into a ciliated airway epithelial cell.[42] For entry inhibitors, Calu-3 is a better model than Vero and A549 cells because Calu-3 expresses TMPRSS2. The lack of antiviral activity of chloroquine in Calu-3 cells would likely have anticipated its failure in clinical trials.[100] Under regular cell culture, Calu-3 and Caco-2 better support virus entry than A549;[89,101] however, the latter are much easier to grow, reinforcing the interest in generating A549-ACE2 cells which replicate SARS-CoV-2 to titers of ~10^7 PFU/mL.

CONCLUSIONS

In conclusion, this study shows the importance of an exhaustive comparison of different cell lines when testing small molecules as inhibitors of SARS-CoV-2 and clearly indicates how subtle differences in experimental approaches with the same cell lines can have dramatic effects on whether a drug is identified as an inhibitor or not. We illustrate this now for Vero cells which when infected with Ebola or SARS-CoV-2 are insensitive to quinacrine, tilorone, and pyronaridine.[58] This may be related to the mechanism of entry in these cells, the lack of IFNs in Vero cells, or other factors that limit activity for these lysosomotropic compounds.[56] While they are not as potent inhibitors against SARS-CoV-2 as remdesivir in most cell types, they are comparable in the A549-ACE2 cell line. Future work will focus on testing the efficacy of these drugs against SARS-CoV-2 in animal models and further interrogation of the mechanism.

METHODS

Chemicals and Reagents. Pyronaridine tetraphosphate [4-[(7-chloro-2-methoxybenzo[*b*][1,5]naphthyridin-10-yl)-amino]-2,6-bis(1-pyrrolidinylmethyl)phenol phosphate (1:4)][54] was purchased from BOC Sciences (Shirley NY). Tilorone and quinacrine were purchased from Cayman Chemicals (Ann Arbor, Michigan). The purity of these compounds is greater than 95%.

Cell Assays. *Vero E6 Cells.* All drugs were tested with Vero E6 cells as described recently.[102] Cells were plated in opaque 96-well plates 1 day prior to infection. Drug stocks were made in dimethyl sulfoxide (DMSO), water, or methanol. Drugs were diluted from the stock to 50 μM and an eight-point 1:2 dilution series made. Cells were pretreated with the drug for 2 h at 37 °C and 5% CO_2 prior to infection at an MOI of 0.01 or 0.004. Vehicle controls were used on every plate, and all treatments were performed in triplicate for each screen. In addition to plates that were infected, parallel plates were left uninfected to monitor cytotoxicity of the drug alone. Three independent screens with this setup were performed. Cells were incubated at 37 °C and 5% CO_2 for 3 days before CellTiter-Glo assays were performed as per the manufacturer's instructions (Promega). Luminescence was read using a Molecular Devices SpectraMax L plate reader.

Vero 76 Cell Reduction of the Virus-Induced Cytopathic Effect (Primary CPE Assay). Confluent or near-confluent cell culture monolayers of Vero 76 cells are prepared in 96-well disposable microplates the day before testing. Cells are maintained in the minimum essential medium (MEM) supplemented with 5% fetal bovine serum (FBS). For antiviral assays, the same medium is used but with FBS reduced to 2% and supplemented with 50 μg/mL gentamicin. Compounds are dissolved in DMSO, saline, or the diluent requested by the submitter. Less soluble compounds are vortexed, heated, and sonicated, and if they still do not go into the solution, they are tested as colloidal suspensions. The test compound is prepared at four serial $\log_{10}$ concentrations, usually 0.1, 1.0, 10, and 100 μg/mL or μM (as per the sponsor's preference). Lower concentrations are used when an insufficient compound is supplied. Five microwells are used per dilution: three for infected cultures and two for uninfected toxicity cultures. Controls for the experiment consist of six microwells that are infected and not treated (virus controls) and six that are untreated and uninfected (cell controls) on every plate. A known active drug is tested in parallel as a positive control drug using the same method as is applied for test compounds. The positive control is tested with every test run.

Growth media are removed from the cells, and the test compound is applied in a 0.1 mL volume to wells at a 2× concentration. The virus, normally at an ~60 $CCID_{50}$ (50% cell culture infectious dose) in a 0.1 mL volume is added to the wells designated for virus infection. The medium devoid of the virus is placed in toxicity control wells and cell control wells. Plates are incubated at 37 °C with 5% CO_2 until marked CPE (>80% CPE for most virus strains) is observed in virus control wells. The plates are then stained with 0.011% neutral red for approximately 2 h at 37 °C in a 5% CO_2 incubator. The neutral red medium is removed by complete aspiration, and the cells may be rinsed 1× with phosphate-buffered solution (PBS) to remove the residual dye. PBS is completely removed, and the incorporated neutral red is eluted with 50% Sorensen's citrate buffer/50% ethanol for at least 30 min. The neutral red dye penetrates living cells; thus, the more intense the red color, the larger the number of viable cells present in the wells. The dye content in each well is quantified using a spectrophotometer at a 540 nm wavelength. The dye content in each set of wells is converted to a percentage of the dye present in untreated control wells using a Microsoft Excel computer-based spreadsheet and normalized based on the virus control. The 50% effective (EC_{50}, virus-inhibitory) concentrations and 50% cytotoxic (CC_{50}, cell-inhibitory) concentrations are then calculated by regression analysis. The quotient of CC_{50} divided by EC_{50} gives the SI value. Compounds showing SI values $\geq$ 10 are considered active.

Vero 76 Cell Reduction of Virus Yield (Secondary VYR Assay). Active compounds are further tested in a confirmatory assay. This assay is set up like the methodology described above, and only eight half-$\log_{10}$ concentrations of the inhibitor are tested for antiviral activity and cytotoxicity. After sufficient virus replication occurs (3 days for SARS-CoV-2), a sample of the supernatant is taken from each infected well (three replicate wells are pooled) and tested immediately or held frozen at −80 °C for later virus titer determination. After maximum CPE is observed, the viable plates are stained with the neutral red dye. The incorporated dye content is quantified as described above to generate the EC_{50} and CC_{50} values. The VYR test is a direct determination of how much the test compound inhibits virus replication. The virus yielded in the presence of the test compound is titrated and compared to virus titers from the untreated virus controls. Samples were collected 3 days after infection. Titration of the viral samples (collected as described in the paragraph above) is performed by endpoint dilution.[103] Serial 1/10 dilutions of the virus are made and plated into four replicate wells containing fresh cell monolayers of Vero 76 cells. Plates are then incubated, and cells are scored for the presence or absence of the virus after distinct CPE is observed (3 days after infection); the $CCID_{50}$ is calculated using the Reed−Muench method.[103] The 90% (one $\log_{10}$) effective concentration (EC_{90}) is calculated by regression analysis by plotting the $\log_{10}$ of the inhibitor concentration versus $\log_{10}$ of the virus produced at

https://dx.doi.org/10.1021/acsomega.0c05996
ACS Omega 2021, 6, 7454−7468

each concentration. Dividing EC_{90} by the CC_{50} gives the SI value for this test.

Yield-Reduction Assays in Monocytes, Calu-3, and Huh-7. Human hepatoma lineage (Huh-7), the lung epithelial cell line (Calu-3), or human primary monocytes from healthy donors ($5 \times 10 \times 10^5$ cell/well in 24-multiwell plates) were infected at an MOI of 0.1 for 1 h at 37 °C and treated with different concentrations of the compounds. Lysis of the cell monolayer was performed 24 h (for monocytes) or 48 h (for Huh-7 and Calu-3 cells) post infection, and the culture supernatant was harvested 48 h post infection; the virus was titrated by PFU assays in Vero E6 cells. Alternatively, cell-associated viral genomic (ORF1b) and subgenomic (ORFE) RNA was quantified by RT-PCR.[104] The standard curve method was employed for virus quantification. For reference to the cell amounts used, the housekeeping gene RNAse P was amplified.[41]

Calu-3 Cells. Calu-3 (ATCC, HTB-55) cells were pretreated with test compounds for 2 h prior to continuous infection with SARS-CoV-2 (isolate USA WA1/2020) at an MOI of 0.5. 48 h post infection, cells were fixed, immunostained, and imaged by automated microscopy for infection (dsRNA + cells/total cell number) and cell number. Sample well data were normalized to aggregated DMSO control wells and plotted versus drug concentration to determine the IC_{50} (infection: blue) and CC_{50} (toxicity: green).

Caco-2 Cell Virus Yield Reduction. For the Caco-2 VYR assay, the methodology is identical to the Vero 76 cell assay other than the insufficient CPE observed on Caco-2 cells to allow EC50 calculations. The supernatant from the Caco-2 cells is collected on day 3 post infection and titrated on Vero 76 cells for virus titer as before.

A549-ACE2 Cells. A549-ACE2 cells were plated in Corning black-walled clear bottom 96-well plates 24 h before infection for confluency. Drug stocks were diluted in DMSO for a 200× concentration in an eight-point 1:4 dilution series. Prepared 200× dilutions were then diluted to a 2× concentration in infection media [Gibco Dulbecco's modified Eagle's medium (DMEM) supplemented with 5% HyClone FetalCloneII, 1% Gibco NEAA, 1% Gibco Pen-Strep]. Growth media were removed, and cells were pretreated with a 2× drug for 1 h prior to infection at 37 °C and 5% CO_2. Cells were either infected at an MOI of 0.02 with the infectious clone SARS-CoV-2-nLuc[97] or mock-infected with infection media to evaluate toxicity. Effects of compounds to the virus were also evaluated by incubating the virus at an MOI of 0.02 with compounds 1 h prior to the infection step. In this step, cell media were removed and 1× of the virus at an MOI of 0.02 was added to the cells. 48 h post infection, wells were treated with Nano-Glo luciferase assay activity to measure viral growth or the CytoTox-Glo Cytotoxicity assay to evaluate toxicity of drug treatments, performed as per the manufacturer's instructions (Promega). Nano-Glo assays were read using a Molecular Devices SpectraMax plate reader, and CytoTox-Glo assays were read using a Promega GloMax plate reader. Vehicle-treated wells on each plate were used to normalize replication and toxicity. Drug treatment was performed in technical duplicate and biological triplicate.

VSV-Pseudotype SARS-CoV-2 Neutralization Assays. Tilorone dihydrochloride, quinacrine hydrochloride, and pyronaridine tetraphosphate were tested for neutralization activity against the SARS-CoV-2 spike protein using a VSV-pseudotyped (rVSV-SARS-CoV-2 S) neutralization assay in Vero ATCC CCL-81 [IBT Bioscience (Rockville, MD)]. The luciferase-based microneutralization assay was conducted in Vero cells seeded in black 96-well plates on day 1 at 6.00×10^4 cells per well. Eight serial dilutions were prepared in triplicate and incubated for 1 h with approximately 10,000 RLU of rVSV-SARS-CoV-2; the virus only and cells only were added for controls and calculations. The TA/virus mixture was then added to the Vero cells, and the plates were incubated for 24 h at 37 °C. Firefly luciferase activity was detected using the Bright-Glo Assay System kit (Promega). The 50% inhibition concentration (IC_{50}) was calculated using the XLfit dose response model.

Murine Hepatitis Virus. Each compound was tested for antiviral activity against MHV, a group 2a betacoronavirus, in DBT cells. Each compound was tested against MHV using an eight-point dose response curve consisting of serial 4-fold dilutions, starting at 10 μM. Cytotoxicity of these compounds was not performed in this cell line, and there was no discernible cytotoxic effect of the compounds at the dosages tested.

HCoV 229E Antiviral Assay. HCoV 229E (a gift from Ralph Baric, UNC, Chapel Hill) was propagated on Huh-7 cells, and titers were determined by the $TCID_{50}$ assay on Huh-7 cells. Huh-7 cells were plated at a density of 25,000 cells per well in 96-well plates and incubated for 24 h at 37 °C and 5% CO_2. Cells were infected with HCoV 229E at an MOI of 0.1 in a volume of 50 μL of MEM 1 + 1 + 1 [modified Eagle's medium, 1% FBS, 1% antibiotics, 1% *N*-(2-hydroxyethyl)piperazine-*N*′-ethanesulfonic acid (HEPES) buffer] for 1 h. The virus was removed, cells were rinsed once with PBS, and compounds were added at the indicated concentrations in a volume of 100 μL. Supernatants were harvested after 24 h, which were serially 10-fold diluted, and virus titer was determined by the $TCID_{50}$ assay on Huh-7 cells. CPE was monitored by visual inspection at 96 h post infection. $TCID_{50}$ titers were calculated using the Spearmann-Karber method.[105,106]

Cytotoxicity. Cytotoxicity of compounds was assessed by the 3-(4,5-dimethylthiazol-2-yl)-2,5-diphenyltetrazolium bromide (MTT) assay for quantification of cellular mitochondrial activity as an indirect measurement of cell viability. Briefly, freshly collected peripheral blood mononuclear cells were plated in a 96-well plate at a concentration of 10^5 cells/well in the RPMI medium for 2 h to allow adhesion of monocytes. The RPMI medium was then changed for a complete medium supplemented with proper drug concentrations and controls for 24 h at 5% CO_2 and 37 °C. Vero CCL81 cells were cultivated at 5% CO_2 and 37 °C using DMEM supplemented with 10% heat-inactivated FBS. For this experiment, Vero cells were seeded at a density of 10^4 cells/well in a 96-well plate prior to incubation with a serial dilution of compounds of interest and controls for 72 h. After drug treatment, cells were next incubated with MTT (Sigma-Aldrich M5655) for 4 h, followed by formazan crystal solubilization with isopropanol and absorbance readings at OD_{570}.[107] Cellular viability was expressed as a percentage relative to the vehicle-treated control. The CC_{50} was defined as the concentration that reduced the absorbance of treated cells to 50% when compared to non-treated controls. For Huh-7 cells, the cytotoxicity of extracts and pure compounds was determined according to the manufacturer's instructions using the CytoScan LDH cytotoxicity assay (G-Biosciences, St. Louis, MO). Briefly, 25,000 Huh-7 cells per well were added to 96-well plates and incubated for 24 h at 37 °C and 5% CO_2. Compounds were added with fresh media at the indicated concentrations to triplicate wells for 24 h. Following the incubation, the plates were centrifuged at 250*g* for 5 min and 50 μL of the supernatant from each well was transferred to a new plate. An equal volume

https://dx.doi.org/10.1021/acsomega.0c05996
ACS Omega 2021, 6, 7454−7468

of the substrate mix was added to each well and the plates incubated at room temperature for 30 m. Then, the stop solution was added, and the absorbance was measured at 490 nm using a plate reader (Synergy HT, BioTek, Winooski, VT). The percent cytotoxicity was determined using the following formula: (experimental-spontaneous absorbance/maximum-spontaneous absorbance) × 100.

Expression and Purification of the Spike RBD of SARS-CoV-2. A codon-optimized gene encoding for SARS-CoV-2 (331−528 amino acids, QIS60558.1) was expressed in Expi293 cells (Thermo Fisher Scientific) with human serum albumin secretion signal sequence and fusion tags (6× Histidine tag, Halo tag, and TwinStrep tag) as described before.[108] The S1 RBD was purified from the culture supernatant by nickel−nitrilotriacetic acid agarose (Qiagen), and the purity was confirmed to be >95% as judged by coomassie-stained sodium dodecyl sulfate-polyacrylamide gel electrophoresis. The purified RBD protein was buffer-exchanged to 1× PBS prior to analysis by MST.

Microscale Thermophoresis. Experiments were performed using a Monolith Pico (NanoTemper). Briefly, 10 μM protein was labeled using a Monolith Protein Labeling Kit RED-NHS 2nd Generation (Amine Reactive), with threefold excess NHS dye in PBS (pH 7.4). The free dye was removed according to the manufacturer's instruction, and the protein was eluted in the MST buffer [*N*-(2-hydroxyethyl)piperazine-*N*′-ethanesulfonic acid (HEPES) 10 mM pH 7.4, NaCl 150 mM] and centrifuged at 15 k rcf for 10 min. Binding affinity measurements were performed using 5 nM protein a serial dilution of compounds, starting at 250 μM. For each experimental compound, 16 independent stocks were made in DMSO using a 2-fold serial dilution (10 mM initial concentration). 19.5 μL of the spike RBD (5 nM) of the labeled protein in the MST buffer containing 0.1% Triton X-100 and 1 mM β-mercaptoethanol (BME) was combined with 0.5 μL of the compound stock and then mixed thoroughly. This resulted in 2-fold serial dilution testing series with the highest and lowest concentrations of 250 μM and 7.629 nM, respectively, with a consistent final DMSO concentration of 2.5%. The protein was incubated on ice in the presence of compounds for 1 h prior to transferring to standard Monolith NT.115 capillaries. Experiments were run at 20% excitation and a high MST power at 23.0 °C on a Monolith NT.115Pico (NanoTemper). Each experimental compound was run in triplicate.

The data were obtained with MO.Control 1.6.1 (NanoTemper Technologies). Recorded data were analyzed with MO.Affinity Analysis 2.3 (NanoTemper Technologies). The dissociation constant K_d quantifies the equilibrium of the reaction of the labeled molecule A (concentration c_A) with its target T (concentration c_T) to form the complex AT (concentration c_{AT}) and is defined by the law of mass action as $K_d = c_A x c_T / c_{AT}$, where all concentrations are "free" concentrations. During the titration experiments, the concentration of the labeled molecule A is kept constant and the concentration of added target T is increased. These concentrations are known and can be used to calculate the dissociation constant. The free concentration of the labeled molecule A is the added concentration minus the concentration of the formed complex AT. The K_d is calculated as $K_d = \frac{(c_A^0 - c_{AT}) x (c_t^0 - c_{AT})}{c_{AT}}$. The fraction of bound molecules x can be derived from F_{norm}, where F_{norm}(A) is the normalized fluorescence of only unbound labeled molecules A and F_{norm}(AT) is the normalized fluorescence of complexes AT labeled as shown by the equation $x = \frac{F_{norm}(c_T^0) - F_{norm}(A)}{F_{norm}(AT) - F_{norm}(A)}$. The MST traces that showed aggregation or outliers were removed from the data sets prior to K_d determination.

■ ASSOCIATED CONTENT

Supporting Information

The Supporting Information is available free of charge at https://pubs.acs.org/doi/10.1021/acsomega.0c05996.

Additional cell testing; pseudovirus testing and pharmacokinetics; and previous *in vitro* and *in vivo* data for quinacrine, tilorone, and pyronaridine (PDF)

■ AUTHOR INFORMATION

Corresponding Authors

Ana C. Puhl − *Collaborations Pharmaceuticals, Inc., Raleigh, North Carolina 27606, United States;* orcid.org/0000-0002-1456-8882; Email: ana@collaborationspharma.com

Sean Ekins − *Collaborations Pharmaceuticals, Inc., Raleigh, North Carolina 27606, United States;* orcid.org/0000-0002-5691-5790; Phone: +1 215-687-1320; Email: sean@collaborationspharma.com

Authors

Ethan J. Fritch − *Department of Microbiology and Immunology, University of North Carolina School of Medicine, Chapel Hill, North Carolina 27599, United States*

Thomas R. Lane − *Collaborations Pharmaceuticals, Inc., Raleigh, North Carolina 27606, United States*

Longping V. Tse − *Department of Epidemiology, University of North Carolina School of Medicine, Chapel Hill, North Carolina 27599, United States*

Boyd L. Yount − *Department of Epidemiology, University of North Carolina School of Medicine, Chapel Hill, North Carolina 27599, United States*

Carolina Q. Sacramento − *Laboratório de Imunofarmacologia, Instituto Oswaldo Cruz (IOC), Fundação Oswaldo Cruz (Fiocruz), Rio de Janeiro, RJ 21040-900, Brazil; Centro De Desenvolvimento Tecnológico Em Saúde (CDTS), Fiocruz, Rio de Janeiro 21040-900, Brazil*

Natalia Fintelman-Rodrigues − *Laboratório de Imunofarmacologia, Instituto Oswaldo Cruz (IOC), Fundação Oswaldo Cruz (Fiocruz), Rio de Janeiro, RJ 21040-900, Brazil; Centro De Desenvolvimento Tecnológico Em Saúde (CDTS), Fiocruz, Rio de Janeiro 21040-900, Brazil*

Tatyana Almeida Tavella − *Laboratory of Tropical Diseases—Prof. Dr. Luiz Jacinto da Silva, Department of Genetics, Evolution, Microbiology and Immunology, University of Campinas-UNICAMP, São Paulo 13083-970, Brazil*

Fabio Trindade Maranhão Costa − *Laboratory of Tropical Diseases—Prof. Dr. Luiz Jacinto da Silva, Department of Genetics, Evolution, Microbiology and Immunology, University of Campinas-UNICAMP, São Paulo 13083-970, Brazil;* orcid.org/0000-0001-9969-7300

Stuart Weston − *Department of Microbiology and Immunology, University of Maryland School of Medicine, Baltimore, Maryland 21201, United States*

James Logue − *Department of Microbiology and Immunology, University of Maryland School of Medicine, Baltimore, Maryland 21201, United States;* orcid.org/0000-0002-7410-9741

https://dx.doi.org/10.1021/acsomega.0c05996
ACS Omega 2021, 6, 7454−7468

Matthew Frieman − *Department of Microbiology and Immunology, University of Maryland School of Medicine, Baltimore, Maryland 21201, United States*
Lakshmanane Premkumar − *Department of Microbiology and Immunology, University of North Carolina School of Medicine, Chapel Hill, North Carolina 27599, United States*
Kenneth H. Pearce − *Center for Integrative Chemical Biology and Drug Discovery, Chemical Biology and Medicinal Chemistry, Eshelman School of Pharmacy, University of North Carolina, Chapel Hill, North Carolina 27599, United States; UNC Lineberger Comprehensive Cancer Center, Chapel Hill, North Carolina 27599, United States*
Brett L. Hurst − *Institute for Antiviral Research, Utah State University, Logan, Utah 84322, United States; Department of Animal, Dairy and Veterinary Sciences, Utah State University, Logan, Utah 84322, United States*
Carolina Horta Andrade − *Laboratory of Tropical Diseases—Prof. Dr. Luiz Jacinto da Silva, Department of Genetics, Evolution, Microbiology and Immunology, University of Campinas-UNICAMP, São Paulo 13083-970, Brazil; LabMol—Laboratory of Molecular Modeling and Drug Design, Faculdade de Farmácia, Universidade Federal de Goiás, Goiânia, GO 74605-170, Brazil*
James A. Levi − *Department of Biological Sciences, North Carolina State University, Raleigh, North Carolina 27695, United States*
Nicole J. Johnson − *Department of Biological Sciences, North Carolina State University, Raleigh, North Carolina 27695, United States*
Samantha C. Kisthardt − *Department of Biological Sciences, North Carolina State University, Raleigh, North Carolina 27695, United States*
Frank Scholle − *Department of Biological Sciences, North Carolina State University, Raleigh, North Carolina 27695, United States*
Thiago Moreno L. Souza − *Laboratório de Imunofarmacologia, Instituto Oswaldo Cruz (IOC), Fundação Oswaldo Cruz (Fiocruz), Rio de Janeiro, RJ 21040-900, Brazil; Centro De Desenvolvimento Tecnológico Em Saúde (CDTS), Fiocruz, Rio de Janeiro 21040-900, Brazil*
Nathaniel John Moorman − *Department of Microbiology and Immunology, University of North Carolina School of Medicine, Chapel Hill, North Carolina 27599, United States; Center for Integrative Chemical Biology and Drug Discovery, Chemical Biology and Medicinal Chemistry, Eshelman School of Pharmacy, University of North Carolina, Chapel Hill, North Carolina 27599, United States; Rapidly Emerging Antiviral Drug Discovery Initiative, University of North Carolina at Chapel Hill, Chapel Hill, North Carolina 27599, United States*
Ralph S. Baric − *Department of Microbiology and Immunology and Department of Epidemiology, University of North Carolina School of Medicine, Chapel Hill, North Carolina 27599, United States; Rapidly Emerging Antiviral Drug Discovery Initiative, University of North Carolina at Chapel Hill, Chapel Hill, North Carolina 27599, United States*
Peter B. Madrid − *SRI International, Menlo Park, California 94025, United States*

Complete contact information is available at: https://pubs.acs.org/10.1021/acsomega.0c05996

Funding
The authors kindly acknowledge NIH funding, R44GM122196-02A1 from NIGMS (PI: S.E.), 1R43AT010585-01 from NIH/NCCAM, AI142759, and AI108197 to R.S.B., and support from DARPA (HR0011-19-C-0108; PI: P.B.M.) is gratefully acknowledged. FTMC and T.A.T. are supported by FAPESP (grant 2017/18611-7 and grant 2020/05369-6 for FTMC and grant 2019/27626-3 for T.A.T.). Distribution Statement "A" (approved for Public Release, Distribution Unlimited). The views, opinions, and/or findings expressed are those of the author and should not be interpreted as representing the official views or policies of the Department of Defense or the U.S. Government. This project was also supported by the North Carolina Policy Collaboratory at the University of North Carolina at Chapel Hill with funding from the North Carolina Coronavirus Relief Fund established and appropriated by the North Carolina General Assembly. Collaborations Pharmaceuticals, Inc. has utilized the non-clinical and pre-clinical services program offered by the National Institute of Allergy and Infectious Diseases.

Notes
The authors declare the following competing financial interest(s): S.E. is CEO of Collaborations Pharmaceuticals, Inc. A.C.P. and T.R.L. are employees at Collaborations Pharmaceuticals, Inc. Collaborations Pharmaceuticals, Inc. has obtained FDA orphan drug designations for pyronaridine, tilorone and quinacrine for use against Ebola. CPI have also filed a provisional patent for use of these molecules against Marburg and other viruses. Other authors have no conflicts.

■ ACKNOWLEDGMENTS

Victor O. Gawriljuk is kindly acknowledged for helping collate literature data on SARS-CoV-2. The authors graciously thank Dr. Sara Cherry and Dr. David Schultz for the Calu-3 high-content SARS-CoV-2 studies performed by the University of Pennsylvania High-Throughput Screening Core and the Cherry Laboratory. Dr. Mindy Davis and colleagues are gratefully acknowledged for assistance with the NIAID virus screening capabilities.

■ ABBREVIATIONS

BMP, bis(monoacylglycero)phosphate; COVID-19, coronavirus disease; EBOV, Ebola virus; MST, microscale thermophoresis; MERS-CoV, middle east respiratory syndrome coronavirus; ma-EBOV, mouse-adapted EBOV; SARS-CoV-2, severe acute respiratory coronavirus 2

■ REFERENCES

(1) Wu, F.; Zhao, S.; Yu, B.; Chen, Y.-M.; Wang, W.; Song, Z.-G.; Hu, Y.; Tao, Z.-W.; Tian, J.-H.; Pei, Y.-Y.; Yuan, M.-L.; Zhang, Y.-L.; Dai, F.-H.; Liu, Y.; Wang, Q.-M.; Zheng, J.-J.; Xu, L.; Holmes, E. C.; Zhang, Y.-Z. Author Correction: A new coronavirus associated with human respiratory disease in China. *Nature* **2020**, *580*, No. E7.
(2) Coronaviridae Study Group of the International Committee on Taxonomy of, Viruses. The species Severe acute respiratory syndrome-related coronavirus: classifying 2019-nCoV and naming it SARS-CoV-2. *Nat. Microbiol.* **2020**, *5*, 536−544.
(3) Liu, J.; Zheng, X.; Tong, Q.; Li, W.; Wang, B.; Sutter, K.; Trilling, M.; Lu, M.; Dittmer, U.; Yang, D. Overlapping and discrete aspects of the pathology and pathogenesis of the emerging human pathogenic coronaviruses SARS-CoV, MERS-CoV, and 2019-nCoV. *J. Med. Virol.* **2020**, *92*, 491−494.
(4) WHO Naming the coronavirus disease (COVID-2019) and the virus that causes it. https://www.who.int/emergencies/diseases/novel-

coronavirus-2019/technical-guidance/naming-the-coronavirus-disease-(covid-2019)-and-the-virus-that-causes-it (accessed Dec 10, 2020).
(5) Pan, Y.; Guan, H.; Zhou, S.; Wang, Y.; Li, Q.; Zhu, T.; Hu, Q.; Xia, L. Initial CT findings and temporal changes in patients with the novel coronavirus pneumonia (2019-nCoV): a study of 63 patients in Wuhan, China. *Eur. Radiol.* **2020**, *30*, 3306−3309.
(6) Whitcroft, K. L.; Hummel, T. Olfactory Dysfunction in COVID-19: Diagnosis and Management. *JAMA* **2020**, *323*, 2512−2514.
(7) Sungnak, W.; Huang, N.; Huang, N.; Bécavin, C.; Berg, M.; Queen, R.; Litvinukova, M.; Talavera-López, C.; Maatz, H.; Reichart, D.; Sampaziotis, F.; Worlock, K. B.; Yoshida, M.; Barnes, J. L. SARS-CoV-2 entry factors are highly expressed in nasal epithelial cells together with innate immune genes. *Nat Med.* **2020**, *26*, 681−687.
(8) Brann, D. H.; Tsukahara, T.; Weinreb, C.; Lipovsek, M.; Van den Berge, K.; Gong, B.; Chance, R.; Macaulay, I. C.; Chou, H.-j.; Fletcher, R. B.; Das, D.; Street, K.; de Bezieux, H. R.; Choi, Y.-G.; Risso, D.; Dudoit, S.; Purdom, E.; Mill, J.; Hachem, R. A.; Matsunami, H.; Logan, D. W.; Goldstein, B. J.; Grubb, M. S.; Ngai, J.; Datta, S. R. Non-neuronal expression of SARS-CoV-2 entry genes in the olfactory system suggests mechanisms underlying COVID-19-associated anosmia. *Sci. Adv.* **2020**, *6*, No. eabc5801.
(9) World Health Organization. WHO Coronavirus Disease (COVID-19) Dashboard. https://covid19.who.int (accessed Dec 10, 2020).
(10) Mulangu, S.; Dodd, L. E.; Davey, R. T., Jr.; Tshiani Mbaya, O.; Proschan, M.; Mukadi, D.; Lusakibanza Manzo, M.; Nzolo, D.; Tshomba Oloma, A.; Ibanda, A.; Ali, R.; Coulibaly, S.; Levine, A. C.; Grais, R.; Diaz, J.; Lane, H. C.; Muyembe-Tamfum, J.-J.; the PALM Writing Group, P. W.; Sivahera, B.; Camara, M.; Kojan, R.; Walker, R.; Dighero-Kemp, B.; Cao, H.; Mukumbayi, P.; Mbala-Kingebeni, P.; Ahuka, S.; Albert, S.; Bonnett, T.; Crozier, I.; Duvenhage, M.; Proffitt, C.; Teitelbaum, M.; Moench, T.; Aboulhab, J.; Barrett, K.; Cahill, K.; Cone, K.; Eckes, R.; Hensley, L.; Herpin, B.; Higgs, E.; Ledgerwood, J.; Pierson, J.; Smolskis, M.; Sow, Y.; Tierney, J.; Sivapalasingam, S.; Holman, W.; Gettinger, N.; Vallee, D.; Nordwall, J.; Team, P. C. S. A Randomized, Controlled Trial of Ebola Virus Disease Therapeutics. *N. Engl. J. Med.* **2019**, *381*, 2293−2303.
(11) de Wit, E.; Feldmann, F.; Cronin, J.; Jordan, R.; Okumura, A.; Thomas, T.; Scott, D.; Cihlar, T.; Feldmann, H. Prophylactic and therapeutic remdesivir (GS-5734) treatment in the rhesus macaque model of MERS-CoV infection. *Proc. Natl. Acad. Sci. U.S.A.* **2020**, *117*, 6771−6776.
(12) Sheahan, T. P.; Sims, A. C.; Graham, R. L.; Menachery, V. D.; Gralinski, L. E.; Case, J. B.; Leist, S. R.; Pyrc, K.; Feng, J. Y.; Trantcheva, I.; Bannister, R.; Park, Y.; Babusis, D.; Clarke, M. O.; Mackman, R. L.; Spahn, J. E.; Palmiotti, C. A.; Siegel, D.; Ray, A. S.; Cihlar, T.; Jordan, R.; Denison, M. R.; Baric, R. S. Broad-spectrum antiviral GS-5734 inhibits both epidemic and zoonotic coronaviruses. *Sci. Transl. Med.* **2017**, *9*, No. eaal3653.
(13) Pruijssers, A. J.; George, A. S.; Schäfer, A.; Leist, S. R.; Gralinksi, L. E.; Dinnon, K. H., III; Yount, B. L.; Agostini, M. L.; Stevens, L. J.; Chappell, J. D.; Lu, X.; Hughes, T. M.; Gully, K.; Martinez, D. R.; Brown, A. J.; Graham, R. L.; Perry, J. K.; Du Pont, V.; Pitts, J.; Ma, B.; Babusis, D.; Murakami, E.; Feng, J. Y.; Bilello, J. P.; Porter, D. P.; Cihlar, T.; Baric, R. S.; Denison, M. R.; Sheahan, T. P. Remdesivir Inhibits SARS-CoV-2 in Human Lung Cells and Chimeric SARS-CoV Expressing the SARS-CoV-2 RNA Polymerase in Mice. *Cell Rep.* **2020**, *32*, 107940.
(14) Wang, M.; Cao, R.; Zhang, L.; Yang, X.; Liu, J.; Xu, M.; Shi, Z.; Hu, Z.; Zhong, W.; Xiao, G. Remdesivir and chloroquine effectively inhibit the recently emerged novel coronavirus (2019-nCoV) in vitro. *Cell Res.* **2020**, *30*, 269−271.
(15) Wang, Y.; Zhang, D.; Du, G.; Du, R.; Zhao, J.; Jin, Y.; Fu, S.; Gao, L.; Cheng, Z.; Lu, Q.; Hu, Y.; Luo, G.; Wang, K.; Lu, Y.; Li, H.; Wang, S.; Ruan, S.; Yang, C.; Mei, C.; Wang, Y.; Ding, D.; Wu, F.; Tang, X.; Ye, X.; Ye, Y.; Liu, B.; Yang, J.; Yin, W.; Wang, A.; Fan, G.; Zhou, F.; Liu, Z.; Gu, X.; Xu, J.; Shang, L.; Zhang, Y.; Cao, L.; Guo, T.; Wan, Y.; Qin, H.; Jiang, Y.; Jaki, T.; Hayden, F. G.; Horby, P. W.; Cao, B.; Wang, C. Remdesivir in adults with severe COVID-19: a randomised, double-blind, placebo-controlled, multicentre trial. *Lancet* **2020**, *395*, 1569−1578.
(16) Lamb, Y. N. Remdesivir: First Approval. *Drugs* **2020**, *80*, 1355−1363.
(17) Liu, J.; Cao, R.; Xu, M.; Wang, X.; Zhang, H.; Hu, H.; Li, Y.; Hu, Z.; Zhong, W.; Wang, M. Hydroxychloroquine, a less toxic derivative of chloroquine, is effective in inhibiting SARS-CoV-2 infection in vitro. *Cell Discovery* **2020**, *6*, 16.
(18) Boulware, D. R.; Pullen, M. F.; Bangdiwala, A. S.; Pastick, K. A.; Lofgren, S. M.; Okafor, E. C.; Skipper, C. P.; Nascene, A. A.; Nicol, M. R.; Abassi, M.; Engen, N. W.; Cheng, M. P.; LaBar, D.; Lother, S. A.; MacKenzie, L. J.; Drobot, G.; Marten, N.; Zarychanski, R.; Kelly, L. E.; Schwartz, I. S.; McDonald, E. G.; Rajasingham, R.; Lee, T. C.; Hullsiek, K. H. A Randomized Trial of Hydroxychloroquine as Postexposure Prophylaxis for Covid-19. *N. Engl. J. Med.* **2020**, *383*, 517−525.
(19) Roomi, S.; Ullah, W.; Ahmed, F.; Farooq, S.; Sadiq, U.; Chohan, A.; Jafar, M.; Saddique, M.; Khanal, S.; Watson, R.; Boigon, M. Efficacy of Hydroxychloroquine and Tocilizumab in Patients With COVID-19: Single-Center Retrospective Chart Review. *J. Med. Internet Res.* **2020**, *22*, No. e21758.
(20) Guy, R. K.; DiPaola, R. S.; Romanelli, F.; Dutch, R. E. Rapid repurposing of drugs for COVID-19. *Science* **2020**, *368*, 829−830.
(21) Baker, N. C.; Ekins, S.; Williams, A. J.; Tropsha, A. A bibliometric review of drug repurposing. *Drug Discovery Today* **2018**, *23*, 661−672.
(22) Mirabelli, C.; Wotring, J. W.; Zhang, C. J.; McCarty, S. M.; Fursmidt, R.; Frum, T.; Kadambi, N. S.; Amin, A. T.; O'Meara, T. R.; Pretto, C. D.; Spence, J. R.; Huang, J.; Alysandratos, K. D.; Kotton, D. N.; Handelman, S. K.; Wobus, C. E.; Weatherwax, K. J.; Mashour, G. A.; O'Meara, M. J.; Sexton, J. Z., Morphological Cell Profiling of SARS-CoV-2 Infection Identifies Drug Repurposing Candidates for COVID-19. **2020**, bioRxiv:2020.05.27.117184.
(23) Yuan, S.; Chan, J. F. W.; Chik, K. K. H.; Chan, C. C. Y.; Tsang, J. O. L.; Liang, R.; Cao, J.; Tang, K.; Chen, L.-L.; Wen, K.; Cai, J.-P.; Ye, Z.-W.; Lu, G.; Chu, H.; Jin, D.-Y.; Yuen, K.-Y. Discovery of the FDA-approved drugs bexarotene, cetilistat, diiodohydroxyquinoline, and abiraterone as potential COVID-19 treatments with a robust two-tier screening system. *Pharmacol. Res.* **2020**, *159*, 104960.
(24) Han, Y.; Duan, X.; Yang, L.; Nilsson-Payant, B. E.; Wang, P.; Duan, F.; Tang, X.; Yaron, T. M.; Zhang, T.; Uhl, S.; Bram, Y.; Richardson, C.; Zhu, J.; Zhao, Z.; Redmond, D.; Houghton, S.; Nguyen, D.-H. T.; Xu, D.; Wang, X.; Jessurun, J.; Borczuk, A.; Huang, Y.; Johnson, J. L.; Liu, Y.; Xiang, J.; Wang, H.; Cantley, L. C.; tenOever, B. R.; Ho, D. D.; Pan, F. C.; Evans, T.; Chen, H. J.; Schwartz, R. E.; Chen, S. Identification of SARS-CoV-2 inhibitors using lung and colonic organoids. *Nature* **2021**, *589*, 270−275.
(25) Riva, L.; Yuan, S.; Yin, X.; Martin-Sancho, L.; Matsunaga, N.; Pache, L.; Burgstaller-Muehlbacher, S.; De Jesus, P. D.; Teriete, P.; Hull, M. V.; Chang, M. W.; Chan, J. F.; Cao, J.; Poon, V. K.; Herbert, K. M.; Cheng, K.; Nguyen, T. H.; Rubanov, A.; Pu, Y.; Nguyen, C.; Choi, A.; Rathnasinghe, R.; Schotsaert, M.; Miorin, L.; Dejosez, M.; Zwaka, T. P.; Sit, K. Y.; Martinez-Sobrido, L.; Liu, W. C.; White, K. M.; Chapman, M. E.; Lendy, E. K.; Glynne, R. J.; Albrecht, R.; Ruppin, E.; Mesecar, A. D.; Johnson, J. R.; Benner, C.; Sun, R.; Schultz, P. G.; Su, A. I.; Garcia-Sastre, A.; Chatterjee, A. K.; Yuen, K. Y.; Chanda, S. K. Discovery of SARS-CoV-2 antiviral drugs through large-scale compound repurposing. *Nature* **2020**, *586*, 113−119.
(26) Jeon, S.; Ko, M.; Lee, J.; Choi, I.; Byun, S. Y.; Park, S.; Shum, D.; Kim, S. Identification of antiviral drug candidates against SARS-CoV-2 from FDA-approved drugs. *Antimicrob. Agents Chemother.* **2020**, *64*, No. e00819-20.
(27) Jin, Z.; Du, X.; Xu, Y.; Deng, Y.; Liu, M.; Zhao, Y.; Zhang, B.; Li, X.; Zhang, L.; Peng, C.; Duan, Y.; Yu, J.; Wang, L.; Yang, K.; Liu, F.; Jiang, R.; Yang, X.; You, T.; Liu, X.; Yang, X.; Bai, F.; Liu, H.; Liu, X.; Guddat, L. W.; Xu, W.; Xiao, G.; Qin, C.; Shi, Z.; Jiang, H.; Rao, Z.; Yang, H. Structure of Mpro from SARS-CoV-2 and discovery of its inhibitors. *Nature* **2020**, *582*, 289−293.
(28) Gawriljuk, V. O.; Kyaw Zin, P. P.; Foil, D. H.; Bernatchez, J.; Beck, S.; Beutler, N.; Ricketts, J.; Yang, L.; Rogers, T.; Puhl, A. C.; Zorn,

https://dx.doi.org/10.1021/acsomega.0c05996
ACS Omega 2021, 6, 7454−7468

K. M.; Lane, T. R.; Godoy, A. S.; Oliva, G.; Siqueira-Neto, J. L.; Madrid, P. B.; Ekins, S. Machine Learning Models Identify Inhibitors of SARS-CoV-2. **2020**, bioRxiv:2020.06.16.154765.
(29) Lane, T. R.; Comer, J. E.; Freiberg, A. N.; Madrid, P. B.; Ekins, S. Repurposing Quinacrine against Ebola Virus InfectionIn Vivo. *Antimicrob. Agents Chemother.* **2019**, *63*, No. e01142-19.
(30) Lane, T. R.; Massey, C.; Comer, J. E.; Anantpadma, M.; Freundlich, J. S.; Davey, R. A.; Madrid, P. B.; Ekins, S. Repurposing The Antimalarial Pyronaridine Tetraphosphate To Protect Against Ebola Virus Infection. *PLoS Neglected Trop. Dis.* **2019**, *13*, No. e0007890.
(31) Ekins, S.; Lingerfelt, M. A.; Comer, J. E.; Freiberg, A. N.; Mirsalis, J. C.; O'Loughlin, K.; Harutyunyan, A.; McFarlane, C.; Green, C. E.; Madrid, P. B. Efficacy of Tilorone Dihydrochloride against Ebola Virus Infection. *Antimicrob. Agents Chemother.* **2018**, *62*, No. e01711-17.
(32) Ekins, S.; Lane, T. R.; Madrid, P. B. Tilorone: a Broad-Spectrum Antiviral Invented in the USA and Commercialized in Russia and beyond. *Pharm. Res.* **2020**, *37*, 71.
(33) Lane, T. R.; Ekins, S. Toward the Target: Tilorone, Quinacrine, and Pyronaridine Bind to Ebola Virus Glycoprotein. *ACS Med. Chem. Lett.* **2020**, *11*, 1653−1658.
(34) Browning, D. J. Pharmacology of Chloroquine and Hydroxychloroquine. *Hydroxychloroquine and chloroquine retinopathy*; Springer, 2014; pp 35−63.
(35) Valdés, A. F.-C. Acridine and acridinones: old and new structures with antimalarial activity. *Open Med. Chem. J.* **2011**, *5*, 11−20.
(36) Gupta, D. K.; Gieselmann, V.; Hasilik, A.; von Figura, K. Tilorone acts as a lysosomotropic agent in fibroblasts. *Hoppe Seylers Z. Physiol. Chem.* **1984**, *365*, 859−866.
(37) Bailly, C. Pyronaridine: An update of its pharmacological activities and mechanisms of action. *Biopolymers* **2020**, No. e23398.
(38) Lane, T. R.; Comer, J. E.; Freiberg, A. N.; Madrid, P. B.; Ekins, S. Repurposing Quinacrine against Ebola Virus Infection. *Antimicrob. Agents Chemother.* **2019**, *63*, No. e01142-19.
(39) Lane, T. R.; Massey, C.; Comer, J. E.; Freiberg, A. N.; Zhou, H.; Dyall, J.; Holbrook, M. R.; Anantpadma, M.; Davey, R. A.; Madrid, P. B.; Ekins, S. Pyronaridine tetraphosphate efficacy against Ebola virus infection in guinea pig. *Antiviral Res.* **2020**, *181*, 104863.
(40) Ekins, S.; Madrid, P. B. Tilorone, a Broad-Spectrum Antiviral for Emerging Viruses. *Antimicrob. Agents Chemother.* **2020**, *64*, No. e00440-20.
(41) Sacramento, C. Q.; Fintelman-Rodrigues, N.; Temerozo, J. R.; de Paula Dias Da Silva, A.; da Silva Gomes Dias, S.; dos Santos da Silva, C.; Ferreira, A. C.; Mattos, M.; Pão, C. R. R.; de Freitas, C. S.; Soares, V. C.; Hoelz, L. V. B.; Fernandes, T. V. A.; Branco, F. S. C.; Bastos, M. M.; Boechat, N.; Saraiva, F. B.; Ferreira, M. A.; Rajoli, R. K. R.; Pedrosa, C. S. G.; Vitória, G.; Souza, L. R. Q.; Goto-Silva, L.; Guimarães, M. Z.; Rehen, S. K.; Owen, A.; Bozza, F. A.; Bou-Habib, D. C.; Bozza, P. T.; Souza, T. M. L. The in vitro antiviral activity of the anti-hepatitis C virus (HCV) drugs daclatasvir and sofosbuvir against SARS-CoV-2. **2020**, bioRxiv:2020.06.15.153411.
(42) Yoshikawa, T.; Hill, T.; Li, K.; Peters, C. J.; Tseng, C.-T. K. Severe acute respiratory syndrome (SARS) coronavirus-induced lung epithelial cytokines exacerbate SARS pathogenesis by modulating intrinsic functions of monocyte-derived macrophages and dendritic cells. *J. Virol.* **2009**, *83*, 3039−3048.
(43) Yount, B.; Denison, M. R.; Weiss, S. R.; Baric, R. S. Systematic assembly of a full-length infectious cDNA of mouse hepatitis virus strain A59. *J. Virol.* **2002**, *76*, 11065−11078.
(44) Corman, V. M.; Eckerle, I.; Memish, Z. A.; Liljander, A. M.; Dijkman, R.; Jonsdottir, H.; Juma Ngeiywa, K. J. Z.; Kamau, E.; Younan, M.; Al Masri, M.; Assiri, A.; Gluecks, I.; Musa, B. E.; Meyer, B.; Müller, M. A.; Hilali, M.; Bornstein, S.; Wernery, U.; Thiel, V.; Jores, J.; Drexler, J. F.; Drosten, C. Link of a ubiquitous human coronavirus to dromedary camels. *Proc. Natl. Acad. Sci. U.S.A.* **2016**, *113*, 9864−9869.
(45) Lim, Y. X.; Ng, Y. L.; Tam, J. P.; Liu, D. X. Human Coronaviruses: A Review of Virus-Host Interactions. *Diseases* **2016**, *4*, 26.
(46) Fehr, A. R.; Perlman, S. Coronaviruses: an overview of their replication and pathogenesis. *Methods Mol. Biol.* **2015**, *1282*, 1−23.
(47) Gan, R.; Rosoman, N. P.; Henshaw, D. J. E.; Noble, E. P.; Georgius, P.; Sommerfeld, N. COVID-19 as a viral functional ACE2 deficiency disorder with ACE2 related multi-organ disease. *Med. Hypotheses* **2020**, *144*, 110024.
(48) Beigel, J. H.; Tomashek, K. M.; Dodd, L. E.; Mehta, A. K.; Zingman, B. S.; Kalil, A. C.; Hohmann, E.; Chu, H. Y.; Luetkemeyer, A.; Kline, S.; Lopez de Castilla, D.; Finberg, R. W.; Dierberg, K.; Tapson, V.; Hsieh, L.; Patterson, T. F.; Paredes, R.; Sweeney, D. A.; Short, W. R.; Touloumi, G.; Lye, D. C.; Ohmagari, N.; Oh, M. D.; Ruiz-Palacios, G. M.; Benfield, T.; Fatkenheuer, G.; Kortepeter, M. G.; Atmar, R. L.; Creech, C. B.; Lundgren, J.; Babiker, A. G.; Pett, S.; Neaton, J. D.; Burgess, T. H.; Bonnett, T.; Green, M.; Makowski, M.; Osinusi, A.; Nayak, S.; Lane, H. C.; Members, A.-S. G. Remdesivir for the Treatment of Covid-19 - Preliminary Report. *N. Engl. J. Med.* **2020**, *383*, 1813−1826.
(49) Krishna, S.; Augustin, Y.; Wang, J.; Xu, C.; Staines, H. M.; Platteeuw, H.; Kamarulzaman, A.; Sall, A.; Kremsner, P. Repurposing Antimalarials to Tackle the COVID-19 Pandemic. *Trends Parasitol.* **2021**, *37*, 8−11.
(50) Bae, J.-Y.; Lee, G. E.; Park, H.; Cho, J.; Kim, Y.-E.; Lee, J.-Y.; Ju, C.; Kim, W.-K.; Kim, J. I.; Park, M.-S. Pyronaridine and artesunate are potential antiviral drugs against COVID-19 and influenza. **2020**, bioRxiv:2020.07.28.225102.
(51) Anon Pyronaridine clinical trials for COVID-19. https://clinicaltrials.gov/ct2/results?cond=Covid19&term=pyronaridine&cntry=&state=&city=&dist= (accessed Dec 10, 2020).
(52) Anon Tilorone clinical trials for COVID-19. https://odessa-journal.com/interchem-started-clinical-trials-for-the-treatment-of-covid-19/ (accessed Dec 10, 2020).
(53) Ekins, S.; Freundlich, J. S.; Clark, A. M.; Anantpadma, M.; Davey, R. A.; Madrid, P. Machine learning models identify molecules active against the Ebola virus in vitro. *F1000Research* **2015**, *4*, 1091.
(54) Zhang, Q.; Chen, C. Z.; Swaroop, M.; Xu, M.; Wang, L.; Lee, J.; Pradhan, M.; Shen, M.; Luo, Z.; Xu, Y.; Huang, W.; Zheng, W.; Ye, Y. Targeting heparan sulfate proteoglycan-assisted endocytosis as a COVID-19 therapeutic option. **2020**, bioRxiv:2020.07.14.202549.
(55) Croft, S. L.; Duparc, S.; Arbe-Barnes, S. J.; Craft, J. C.; Shin, C. S.; Fleckenstein, L.; Borghini-Fuhrer, I.; Rim, H. J. Review of pyronaridine anti-malarial properties and product characteristics. *Malar. J.* **2012**, *11*, 270.
(56) Lane, T. R.; Dyall, J.; Mercer, L.; Goodin, C.; Foil, D. H.; Zhou, H.; Postnikova, E.; Liang, J. Y.; Holbrook, M. R.; Madrid, P. B.; Ekins, S. Repurposing Pyramax, quinacrine and tilorone as treatments for Ebola virus disease. *Antiviral Res.* **2020**, *182*, 104908.
(57) Han, Y.; Yang, L.; Duan, X.; Duan, F.; Nilsson-Payant, B. E.; Yaron, T. M.; Wang, P.; Tang, X.; Zhang, T.; Zhao, Z.; Bram, Y.; Redmond, D.; Houghton, S.; Nguyen, D.; Xu, D.; Wang, X.; Uhl, S.; Huang, Y.; Johnson, J. L.; Xiang, J.; Wang, H.; Pan, F. C.; Cantley, L. C.; tenOever, B. R.; Ho, D. D.; Evans, T.; Schwartz, R. E.; Chen, H. J.; Chen, S. Identification of Candidate COVID-19 Therapeutics using hPSC-derived Lung Organoids. **2020**, bioRxiv:2020.05.05.079095.
(58) Lane, T. R.; Massey, C.; Comer, J. E.; Anantpadma, M.; Freundlich, J. S.; Davey, R. A.; Madrid, P. B.; Ekins, S. Repurposing the antimalarial pyronaridine tetraphosphate to protect against Ebola virus infection. *PLoS Neglected Trop. Dis.* **2019**, *13*, No. e0007890.
(59) Wrapp, D.; Wang, N.; Corbett, K. S.; Goldsmith, J. A.; Hsieh, C.-L.; Abiona, O.; Graham, B. S.; McLellan, J. S. Cryo-EM structure of the 2019-nCoV spike in the prefusion conformation. *Science* **2020**, *367*, 1260−1263.
(60) Chan, K. K.; Dorosky, D.; Sharma, P.; Abbasi, S. A.; Dye, J. M.; Kranz, D. M.; Herbert, A. S.; Procko, E. Engineering human ACE2 to optimize binding to the spike protein of SARS coronavirus 2. *Science* **2020**, *369*, 1261−1265.
(61) Salata, C.; Calistri, A.; Alvisi, G.; Celestino, M.; Parolin, C.; Palu, G. Ebola Virus Entry: From Molecular Characterization to Drug Discovery. *Viruses* **2019**, *11*, 274.
(62) Ghosh, S.; Dellibovi-Ragheb, T. A.; Kerviel, A.; Pak, E.; Qiu, Q.; Fisher, M.; Takvorian, P. M.; Bleck, C.; Hsu, V. W.; Fehr, A. R.; Perlman, S.; Achar, S. R.; Straus, M. R.; Whittaker, G. R.; de Haan, C. A.

https://dx.doi.org/10.1021/acsomega.0c05996
ACS Omega 2021, 6, 7454−7468

M.; Kehrl, J.; Altan-Bonnet, G.; Altan-Bonnet, N. β-Coronaviruses Use Lysosomes for Egress Instead of the Biosynthetic Secretory Pathway. *Cell* **2020**, *183*, 1520−1535.e14.
(63) Castano-Rodriguez, C.; Honrubia, J. M.; Gutierrez-Alvarez, J.; DeDiego, M. L.; Nieto-Torres, J. L.; Jimenez-Guardeno, J. M.; Regla-Nava, J. A.; Fernandez-Delgado, R.; Verdia-Baguena, C.; Queralt-Martin, M.; Kochan, G.; Perlman, S.; Aguilella, V. M.; Sola, I.; Enjuanes, L. Role of Severe Acute Respiratory Syndrome Coronavirus Viroporins E, 3a, and 8a in Replication and Pathogenesis. *mBio* **2018**, *9*, e02325−17.
(64) Lu, W.; Zheng, B.-J.; Xu, K.; Schwarz, W.; Du, L.; Wong, C. K. L.; Chen, J.; Duan, S.; Deubel, V.; Sun, B. Severe acute respiratory syndrome-associated coronavirus 3a protein forms an ion channel and modulates virus release. *Proc. Natl. Acad. Sci. U.S.A.* **2006**, *103*, 12540−12545.
(65) Yue, Y.; Nabar, N. R.; Shi, C. S.; Kamenyeva, O.; Xiao, X.; Hwang, I. Y.; Wang, M.; Kehrl, J. H. SARS-Coronavirus Open Reading Frame-3a drives multimodal necrotic cell death. *Cell Death Dis.* **2018**, *9*, 904.
(66) Yount, B.; Roberts, R. S.; Sims, A. C.; Deming, D.; Frieman, M. B.; Sparks, J.; Denison, M. R.; Davis, N.; Baric, R. S. Severe acute respiratory syndrome coronavirus group-specific open reading frames encode nonessential functions for replication in cell cultures and mice. *J. Virol.* **2005**, *79*, 14909−14922.
(67) Nieva, J. L.; Madan, V.; Carrasco, L. Viroporins: structure and biological functions. *Nat. Rev. Microbiol.* **2012**, *10*, 563−574.
(68) Lu, S.; Sung, T.; Lin, N.; Abraham, R. T.; Jessen, B. A. Lysosomal adaptation: How cells respond to lysosomotropic compounds. *PLoS One* **2017**, *12*, No. e0173771.
(69) Marceau, F.; Bawolak, M.-T.; Lodge, R.; Bouthillier, J.; Gagné-Henley, A.; Gaudreault, R. C.; Morissette, G. Cation trapping by cellular acidic compartments: beyond the concept of lysosomotropic drugs. *Toxicol. Appl. Pharmacol.* **2012**, *259*, 1−12.
(70) Mauthe, M.; Orhon, I.; Rocchi, C.; Zhou, X.; Luhr, M.; Hijlkema, K.-J.; Coppes, R. P.; Engedal, N.; Mari, M.; Reggiori, F. Chloroquine inhibits autophagic flux by decreasing autophagosome-lysosome fusion. *Autophagy* **2018**, *14*, 1435−1455.
(71) Kaufmann, A. M.; Krise, J. P. Niemann-Pick C1 functions in regulating lysosomal amine content. *J. Biol. Chem.* **2008**, *283*, 24584−24593.
(72) Rivinoja, A.; Hassinen, A.; Kokkonen, N.; Kauppila, A.; Kellokumpu, S. Elevated Golgi pH impairs terminalN-glycosylation by inducing mislocalization of Golgi glycosyltransferases. *J. Cell. Physiol.* **2009**, *220*, 144−154.
(73) Chen, P. M.; Gombart, Z. J.; Chen, J. W. Chloroquine treatment of ARPE-19 cells leads to lysosome dilation and intracellular lipid accumulation: possible implications of lysosomal dysfunction in macular degeneration. *Cell Biosci.* **2011**, *1*, 10.
(74) Kellokumpu, S.; Sormunen, R.; Kellokumpu, I. Abnormal glycosylation and altered Golgi structure in colorectal cancer: dependence on intra-Golgi pH. *FEBS Lett.* **2002**, *516*, 217−224.
(75) Matlin, K. S. Ammonium chloride slows transport of the influenza virus hemagglutinin but does not cause mis-sorting in a polarized epithelial cell line. *J. Biol. Chem.* **1986**, *261*, 15172−15178.
(76) Ellis, M. A.; Weisz, O. A. In vitro assays differentially recapitulate protein export from the trans-Golgi network. *Anal. Biochem.* **2006**, *354*, 314−316.
(77) Ravindran, M. S.; Bagchi, P.; Cunningham, C. N.; Tsai, B. Opportunistic intruders: how viruses orchestrate ER functions to infect cells. *Nat. Rev. Microbiol.* **2016**, *14*, 407−420.
(78) Robinson, M.; Schor, S.; Barouch-Bentov, R.; Einav, S. Viral journeys on the intracellular highways. *Cell. Mol. Life Sci.* **2018**, *75*, 3693−3714.
(79) Orogo, A. M.; Choi, S. S.; Minnier, B. L.; Kruhlak, N. L. Construction and Consensus Performance of (Q)SAR Models for Predicting Phospholipidosis Using a Dataset of 743 Compounds. *Mol. Inf.* **2012**, *31*, 725−739.
(80) Shayman, J. A.; Abe, A. Drug induced phospholipidosis: an acquired lysosomal storage disorder. *Biochim. Biophys. Acta* **2013**, *1831*, 602−611.
(81) Baciu, M.; Sebai, S. C.; Ces, O.; Mulet, X.; Clarke, J. A.; Shearman, G. C.; Law, R. V.; Templer, R. H.; Plisson, C.; Parker, C. A.; Gee, A. Degradative transport of cationic amphiphilic drugs across phospholipid bilayers. *Philos. Trans. R. Soc., A* **2006**, *364*, 2597−2614.
(82) Lähdesmäki, K.; Ollila, O. H. S.; Koivuniemi, A.; Kovanen, P. T.; Hyvönen, M. T. Membrane simulations mimicking acidic pH reveal increased thickness and negative curvature in a bilayer consisting of lysophosphatidylcholines and free fatty acids. *Biochim. Biophys. Acta* **2010**, *1798*, 938−946.
(83) Stiasny, K.; Heinz, F. X. Effect of membrane curvature-modifying lipids on membrane fusion by tick-borne encephalitis virus. *J. Virol.* **2004**, *78*, 8536−8542.
(84) Zhu, N.; Zhang, D.; Wang, W.; Li, X.; Yang, B.; Song, J.; Zhao, X.; Huang, B.; Shi, W.; Lu, R.; Niu, P.; Zhan, F.; Ma, X.; Wang, D.; Xu, W.; Wu, G.; Gao, G. F.; Tan, W.; China Novel Coronavirus, I.; Research, T. A Novel Coronavirus from Patients with Pneumonia in China, 2019. *N. Engl. J. Med.* **2020**, *382*, 727−733.
(85) Takayama, K. In Vitro and Animal Models for SARS-CoV-2 research. *Trends Pharmacol. Sci.* **2020**, *41*, 513−517.
(86) Kim, J.-M.; Chung, Y.-S.; Jo, H. J.; Lee, N.-J.; Kim, M. S.; Woo, S. H.; Park, S.; Kim, J. W.; Kim, H. M.; Han, M.-G. Identification of Coronavirus Isolated from a Patient in Korea with COVID-19. *Osong Public Health Res. Perspect* **2020**, *11*, 3−7.
(87) Ou, X.; Liu, Y.; Lei, X.; Li, P.; Mi, D.; Ren, L.; Guo, L.; Guo, R.; Chen, T.; Hu, J.; Xiang, Z.; Mu, Z.; Chen, X.; Chen, J.; Hu, K.; Jin, Q.; Wang, J.; Qian, Z. Characterization of spike glycoprotein of SARS-CoV-2 on virus entry and its immune cross-reactivity with SARS-CoV. *Nat. Commun.* **2020**, *11*, 1620.
(88) Harcourt, J.; Tamin, A.; Lu, X.; Kamili, S.; Sakthivel, S. K.; Murray, J.; Queen, K.; Tao, Y.; Paden, C. R.; Zhang, J.; Li, Y.; Uehara, A.; Wang, H.; Goldsmith, C.; Bullock, H. A.; Wang, L.; Whitaker, B.; Lynch, B.; Gautam, R.; Schindewolf, C.; Lokugamage, K. G.; Scharton, D.; Plante, J. A.; Mirchandani, D.; Widen, S. G.; Narayanan, K.; Makino, S.; Ksiazek, T. G.; Plante, K. S.; Weaver, S. C.; Lindstrom, S.; Tong, S.; Menachery, V. D.; Thornburg, N. J. Isolation and characterization of SARS-CoV-2 from the first US COVID-19 patient. **2020**, bioRxiv:2020.03.02.972935.
(89) Chu, H.; Chan, J. F.-W.; Yuen, T. T.-T.; Shuai, H.; Yuan, S.; Wang, Y.; Hu, B.; Yip, C. C.-Y.; Tsang, J. O.-L.; Huang, X.; Chai, Y.; Yang, D.; Hou, Y.; Chik, K. K.-H.; Zhang, X.; Fung, A. Y.-F.; Tsoi, H.-W.; Cai, J.-P.; Chan, W.-M.; Ip, J. D.; Chu, A. W.-H.; Zhou, J.; Lung, D. C.; Kok, K.-H.; To, K. K.-W.; Tsang, O. T.-Y.; Chan, K.-H.; Yuen, K.-Y. Comparative tropism, replication kinetics, and cell damage profiling of SARS-CoV-2 and SARS-CoV with implications for clinical manifestations, transmissibility, and laboratory studies of COVID-19: an observational study. *Lancet Microbe* **2020**, *1*, e14−e23.
(90) Desmyter, J.; Melnick, J. L.; Rawls, W. E. Defectiveness of interferon production and of rubella virus interference in a line of African green monkey kidney cells (Vero). *J. Virol.* **1968**, *2*, 955−961.
(91) Nwosu, Z. C.; Battello, N.; Rothley, M.; Pioronska, W.; Sitek, B.; Ebert, M. P.; Hofmann, U.; Sleeman, J.; Wolfl, S.; Meyer, C.; Megger, D. A.; Dooley, S. Liver cancer cell lines distinctly mimic the metabolic gene expression pattern of the corresponding human tumours. *J. Exp. Clin. Cancer Res.* **2018**, *37*, 211.
(92) Dittmar, M.; Lee, J. S.; Whig, K.; Segrist, E.; Li, M.; Jurado, K.; Samby, K.; Ramage, H.; Schultz, D.; Cherry, S. Drug repurposing screens reveal FDA approved drugs active against SARS-Cov-2. **2020**, bioRxiv:2020.06.19.161042.
(93) Harrison, A. G.; Lin, T.; Wang, P. Mechanisms of SARS-CoV-2 Transmission and Pathogenesis. *Trends Immunol.* **2020**, *41*, 1100−1115.
(94) Shulla, A.; Heald-Sargent, T.; Subramanya, G.; Zhao, J.; Perlman, S.; Gallagher, T. A transmembrane serine protease is linked to the severe acute respiratory syndrome coronavirus receptor and activates virus entry. *J. Virol.* **2011**, *85*, 873−882.

https://dx.doi.org/10.1021/acsomega.0c05996
ACS Omega 2021, 6, 7454−7468

(95) Shang, J.; Wan, Y.; Luo, C.; Ye, G.; Geng, Q.; Auerbach, A.; Li, F. Cell entry mechanisms of SARS-CoV-2. *Proc. Natl. Acad. Sci. U.S.A.* **2020**, *117*, 11727−11734.
(96) Lukassen, S.; Chua, R. L.; Trefzer, T.; Kahn, N. C.; Schneider, M. A.; Muley, T.; Winter, H.; Meister, M.; Veith, C.; Boots, A. W.; Hennig, B. P.; Kreuter, M.; Conrad, C.; Eils, R. SARS-CoV-2 receptor ACE2 and TMPRSS2 are primarily expressed in bronchial transient secretory cells. *EMBO J.* **2020**, *39*, No. e105114.
(97) Hou, Y. J.; Okuda, K.; Edwards, C. E.; Martinez, D. R.; Asakura, T.; Dinnon, K. H., III; Kato, T.; Lee, R. E.; Yount, B. L.; Mascenik, T. M.; Chen, G.; Olivier, K. N.; Ghio, A.; Tse, L. V.; Leist, S. R.; Gralinski, L. E.; Schäfer, A.; Dang, H.; Gilmore, R.; Nakano, S.; Sun, L.; Fulcher, M. L.; Livraghi-Butrico, A.; Nicely, N. I.; Cameron, M.; Cameron, C.; Kelvin, D. J.; de Silva, A.; Margolis, D. M.; Markmann, A.; Bartelt, L.; Zumwalt, R.; Martinez, F. J.; Salvatore, S. P.; Borczuk, A.; Tata, P. R.; Sontake, V.; Kimple, A.; Jaspers, I.; O'Neal, W. K.; Randell, S. H.; Boucher, R. C.; Baric, R. S. SARS-CoV-2 Reverse Genetics Reveals a Variable Infection Gradient in the Respiratory Tract. *Cell* **2020**, *182*, 429−446.
(98) Carsana, L.; Sonzogni, A.; Nasr, A.; Rossi, R. S.; Pellegrinelli, A.; Zerbi, P.; Rech, R.; Colombo, R.; Antinori, S.; Corbellino, M.; Galli, M.; Catena, E.; Tosoni, A.; Gianatti, A.; Nebuloni, M. Pulmonary post-mortem findings in a series of COVID-19 cases from northern Italy: a two-centre descriptive study. *Lancet Infect. Dis.* **2020**, *20*, 1135−1140.
(99) Wu, J.; Wang, Y.; Liu, G.; Jia, Y.; Yang, J.; Shi, J.; Dong, J.; Wei, J.; Liu, X. Characterization of air-liquid interface culture of A549 alveolar epithelial cells. *Braz. J. Med. Biol. Res.* **2017**, *51*, No. e6950.
(100) Hoffmann, M.; Mösbauer, K.; Hofmann-Winkler, H.; Kaul, A.; Kleine-Weber, H.; Krüger, N.; Gassen, N. C.; Müller, M. A.; Drosten, C.; Pöhlmann, S. Chloroquine does not inhibit infection of human lung cells with SARS-CoV-2. *Nature* **2020**, *585*, 588−590.
(101) Hoffmann, M.; Kleine-Weber, H.; Schroeder, S.; Krüger, N.; Herrler, T.; Erichsen, S.; Schiergens, T. S.; Herrler, G.; Wu, N.-H.; Nitsche, A.; Müller, M. A.; Drosten, C.; Pöhlmann, S. SARS-CoV-2 Cell Entry Depends on ACE2 and TMPRSS2 and Is Blocked by a Clinically Proven Protease Inhibitor. *Cell* **2020**, *181*, 271−280.
(102) Weston, S.; Coleman, C. M.; Haupt, R.; Logue, J.; Matthews, K.; Li, Y.; Reyes, H. M.; Weiss, S. R.; Frieman, M. B. Broad Anti-coronavirus Activity of Food and Drug Administration-Approved Drugs against SARS-CoV-2 In Vitro and SARS-CoV In Vivo. *J. Virol.* **2020**, *94*, e01218−20.
(103) Reed, L. J.; Muench, H. A Simple Method of Estimating Fifty per Cent Endpoints12. *Am. J. Hyg.* **1938**, *27*, 493−497.
(104) Wölfel, R.; Corman, V. M.; Guggemos, W.; Seilmaier, M.; Zange, S.; Müller, M. A.; Niemeyer, D.; Jones, T. C.; Vollmar, P.; Rothe, C.; Hoelscher, M.; Bleicker, T.; Brünink, S.; Schneider, J.; Ehmann, R.; Zwirglmaier, K.; Drosten, C.; Wendtner, C. Virological assessment of hospitalized patients with COVID-2019. *Nature* **2020**, *581*, 465−469.
(105) Spearman, C. The method of 'right and wrong cases' ('constant stimuli') without Gauss's formulae. *Br. J. Psychol* **1908**, *2*, 227−242.
(106) Kärber, G. Beitrag zur kollektiven behandlung pharmakologischer reihenversuche. *Naunyn-Schmiedebergs Arch. Exp. Pathol. Pharmakol.* **1931**, *162*, 480−483.
(107) Kumar, P.; Nagarajan, A.; Uchil, P. D. Analysis of Cell Viability by the MTT Assay. *Cold Spring Harb. Protoc.* **2018**, *2018*, pdb.prot095505.
(108) Premkumar, L.; Segovia-Chumbez, B.; Jadi, R.; Martinez, D. R.; Raut, R.; Markmann, A.; Cornaby, C.; Bartelt, L.; Weiss, S.; Park, Y.; Edwards, C. E.; Weimer, E.; Scherer, E. M.; Rouphael, N.; Edupuganti, S.; Weiskopf, D.; Tse, L. V.; Hou, Y. J.; Margolis, D.; Sette, A.; Collins, M. H.; Schmitz, J.; Baric, R. S.; de Silva, A. M. The receptor binding domain of the viral spike protein is an immunodominant and highly specific target of antibodies in SARS-CoV-2 patients. *Sci. Immunol.* **2020**, *5*, No. eabc8413.

https://dx.doi.org/10.1021/acsomega.0c05996
ACS Omega 2021, 6, 7454−7468